

# Nucleon distribution amplitudes and their application to nucleon form factors and the $N \rightarrow \Delta$ transition at intermediate values of $Q^2$

Alexander Lenz, Meinulf Gökeler, Thomas Kaltenbrunner, and Nikolaus Warkentin

*Fakultät für Physik, Universität Regensburg, 93040 Regensburg, Germany*

(Received 20 March 2009; published 15 May 2009)

We compare a recent lattice determination of the nucleon distribution amplitudes with other approaches and models. We study the nucleon distribution amplitudes up to twist 6 in next-to-leading conformal spin and we also investigate conformal  $d$ -wave contributions to the leading-twist distribution amplitude. With the help of light-cone sum rules one can relate the distribution amplitudes to the form factors of the nucleon or the  $N \rightarrow \Delta$  transition at intermediate values of the momentum transfer. We compare our results with experimental data in the range  $1 \text{ GeV}^2 \leq Q^2 \leq 10 \text{ GeV}^2$ . Keeping in mind that we are working only in leading order QCD and next-to-leading order QCD corrections might be sizeable, we already obtain a surprisingly good agreement for the nucleon form factors  $G_M^N$ ,  $G_M^p$ ,  $G_A^p$ , and  $G_T^p$  and for the  $N \rightarrow \Delta$  transition form factor ratios  $R_{EM}$  and  $R_{SM}$ .

DOI: [10.1103/PhysRevD.79.093007](https://doi.org/10.1103/PhysRevD.79.093007)

PACS numbers: 13.40.Gp, 11.15.Tk, 12.38.Gc

## I. INTRODUCTION

The nucleon distribution amplitudes represent the universal nonperturbative input to numerous exclusive reactions, see, e.g., [1] for an early review. Taking corrections up to twist 6 [2] into account we compare different nonperturbative methods to determine the nucleon distribution amplitudes, in particular, lattice simulations [3–5], QCD sum-rule estimates [2,6], and a phenomenological model [6]. For asymptotically large values of the momentum transfer  $Q^2$  the form factors can be expressed as a convolution of two leading-twist distribution amplitudes with a hard—perturbatively calculable—scattering kernel [7–15]. This approach (pQCD) is formally proven in the  $Q^2 \rightarrow \infty$  limit, and currently there is the consensus that pQCD is not valid at experimentally accessible values of the momentum transfer. In [16] light-cone sum rules (LCSR) [17,18] were worked out which relate the nucleon distribution amplitudes to the experimentally accessible form factors of the nucleon at intermediate momentum transfer. Form factors are interesting quantities *per se*, since they encode information about the structure of the investigated baryon. This interest has risen a lot in recent years, in particular, because new data from JLAB [19–22] for the well-known electromagnetic form factors of the nucleon contradict common textbook wisdom. See, e.g., [23] for a review and further references. To our knowledge light-cone sum rules are the only theoretical approach to determine form factors at intermediate momentum transfer that incorporate consistently the purely perturbative approach (pQCD). This was explicitly shown in the case of the pion form factor [24]. If one calculates the light-cone sum rules for the pion form factor to leading order (LO) and next-to-leading order (NLO) in QCD one can show that the  $\alpha_s$  corrections include the pQCD result in the  $Q^2 \rightarrow \infty$  limit. In the case of baryon form factors the pQCD result is expected to be included in the  $\mathcal{O}(\alpha_s^2)$

corrections to the light-cone sum-rule calculation. Currently only leading-order sum rules for the baryon form factors are known and a part of the NLO-QCD corrections to the nucleon form factors.

The paper is organized as follows. In Sec. II we introduce the concept of distribution amplitudes, in Sec. III we collect QCD sum-rule predictions for the nucleon distribution amplitudes, and in Sec. IV we quickly explain the lattice determination of the moments of the nucleon distribution amplitudes. All these approaches, including the numerical results, are discussed in Sec. V. The light-cone sum-rule formalism is introduced in Sec. VI where we also give a short overview over the current literature on light-cone sum rules for baryonic form factors. In the next three sections we compare light-cone sum-rule predictions with different models of the nucleon distribution amplitude for the form factors of the nucleon and for the  $N \rightarrow \Delta$  transition. In Sec. VII we use the nucleon distribution amplitudes including next-to-leading conformal spin contributions to determine the form factors, in Sec. VIII we make use of some relations between twist-4 and twist-3 parameters, and in Sec. IX we investigate the effect of the  $d$ -wave contributions to the leading-twist distribution amplitude. We conclude and summarize our results in Sec. X.

In the Appendixes we give for the first time the full expression for all nucleon distribution amplitudes up to twist 6 including also the  $d$ -wave contribution for the leading-twist distribution amplitude.

## II. THE NUCLEON DISTRIBUTION AMPLITUDES

The distribution amplitudes comprise the infrared behavior in exclusive processes involving large momentum transfer. They remove the infrared divergences in the perturbative diagrams encoding the nonperturbative content of the process and are defined in terms of the Bethe-Salpeter wave function

$$\Psi_{\text{BS}}(x, k_{\perp}) = \langle 0 | T [q(x_1, k_{1,\perp}) q(x_2, k_{2,\perp}) q(x_3, k_{3,\perp})] | P \rangle \quad (1)$$

with  $x_i$  being the longitudinal momentum fraction carried by the quark  $i$ ,  $k_{i,\perp}$  its transverse momentum, and  $|P\rangle$  the nucleon state with momentum  $P$  ( $P^2 = M_N^2$ ). The distribution amplitudes are then obtained by integrating out the transverse momenta,

$$\Phi(x_i, \mu) = Z(\mu) \int^{|k_{\perp}| \leq \mu} d^2 k_{i,\perp} \Psi_{\text{BS}}(x, k_{\perp}), \quad (2)$$

where  $Z$  results from the renormalization of the quark field operators. In coordinate space the nucleon distribution amplitudes are derived from the following nonlocal nucleon-to-vacuum matrix element (here we follow the definitions in [2])

$$\langle 0 | \epsilon_{ijk} u_{\alpha}^i(a_1 x) [a_1 x, a_0 x]_{i',i} u_{\beta}^j(a_2 x) [a_2 x, a_0 x]_{j',j} d_{\gamma}^k(a_3 x) \times [a_3 x, a_0 x]_{k',k} | P \rangle; \quad (3)$$

$u$  and  $d$  are quark field operators,  $\alpha$ ,  $\beta$ , and  $\gamma$  are Dirac indices, while  $i$ ,  $j$ , and  $k$  are color indices;  $x$  is an arbitrary lightlike vector,  $x^2 = 0$ , while the  $a_i$  are real numbers that fulfill  $a_1 + a_2 + a_3 = 1$ . The gauge factors  $[x, y]$  are defined as

$$[x, y] = \mathcal{P} \exp \left[ ig \int_0^1 dt (x-y)_{\mu} A^{\mu}(tx + (1-t)y) \right], \quad (4)$$

where path ordering  $\mathcal{P}$  is implied. They render the matrix element in Eq. (3) gauge invariant. In the following formulas we omit the gauge factors in order to simplify the notation. The leading-twist contribution to the nucleon distribution amplitudes has been determined a long time ago including terms of next-to-next-to-leading conformal spin; see, e.g., [1] for an early review. We compare different determinations of the arising nonperturbative parameters in Sec. V. Currently the nucleon distribution amplitudes have been expanded up to contributions of twist 6 in [2] and the corresponding nonperturbative parameters were estimated in [2,6] with QCD sum rules and in [6] from a phenomenological model. Some of these parameters were also calculated on the lattice [3–5,25,26]. So-called  $x^2$  corrections [corresponding to deviations from the lightlike separations of the quark fields in Eq. (3)] to the leading-twist distribution amplitudes were determined in [6,16,27,28]; they are formally of twist 5. Using the symmetry properties of the quark fields the matrix element in (3) can be expanded in twist as

$$4 \langle 0 | \epsilon_{ijk} u_{\alpha}^i(a_1 x) u_{\beta}^j(a_2 x) d_{\gamma}^k(a_3 x) | P \rangle = \sum_i (\Gamma_3)_{\alpha\beta}^i (\Gamma_4)_{\gamma}^i F_i, \quad (5)$$

where  $\Gamma_{3/4}$  are certain Dirac structures and the  $F_i$  are distribution amplitudes, which can be expanded into eigenstates of conformal symmetry. This results in terms containing local operators. These local operators are

associated with the moments of the distribution amplitudes, which are defined as

$$F_i^{n_1 n_2 n_3} = \frac{1}{F_{i,N}} \int_0^1 \mathcal{D}x x_1^{n_1} x_2^{n_2} x_3^{n_3} F_i(x_1, x_2, x_3). \quad (6)$$

Here  $F_i(x_1, x_2, x_3)$  stands for a distribution amplitude and  $F_{i,N}$  for its normalization constant, which is chosen such that  $F_i^{000} \equiv 1$ . The integration measure is defined as

$$\mathcal{D}x = dx_1 dx_2 dx_3 \delta(1 - x_1 - x_2 - x_3). \quad (7)$$

Thus momentum conservation implies for the moments of the distribution amplitudes the relation

$$F_i^{n_1 n_2 n_3} = F_i^{(n_1+1) n_2 n_3} + F_i^{n_1 (n_2+1) n_3} + F_i^{n_1 n_2 (n_3+1)}. \quad (8)$$

Further details on distribution amplitudes (with complete expressions and definitions up to twist 6) are summarized in the Appendixes. For the nucleon distribution amplitudes isospin symmetry and the presence of two quarks of the same type implies that the number of independent distribution amplitudes is reduced compared to the general case. In particular, the leading-twist nucleon distribution amplitudes can be expressed in terms of only one independent distribution amplitude which is usually taken as

$$\varphi(x_1, x_2, x_3) = V_1(x_1, x_2, x_3) - A_1(x_1, x_2, x_3) \quad (9)$$

and is equal to  $\Phi_3(x_1, x_2, x_3)$  in the notation of [2]. The distribution amplitudes  $A_1$  and  $V_1$  are defined in the Appendixes. At leading twist the nucleon distribution amplitude  $\varphi(x_i)$  corresponds to the following form of the proton state [29,30]:

$$|P, \uparrow\rangle = \int_0^1 \mathcal{D}x \frac{\varphi(x_i)}{\sqrt{96 x_1 x_2 x_3}} |u^l(x_1) [u^l(x_2) d^l(x_3) - d^l(x_2) u^l(x_3)]\rangle. \quad (10)$$

The first moments of  $\varphi(x_i)$  can be interpreted as the momentum fractions carried by the quarks.

The leading-twist distribution amplitude depends at leading conformal spin on one nonperturbative parameter, the normalization constant  $f_N$ , while for twist 4 we have two additional constants  $\lambda_1$  and  $\lambda_2$ . In our approach no new parameters appear in leading conformal spin up to twist 6. At next-to-leading conformal spin only two nonperturbative parameters  $V_1^d = \varphi^{001}$  and  $A_1^u = \varphi^{100} - \varphi^{010}$  arise in the case of leading twist and at next-to-leading twist we have three nonperturbative parameters,  $f_1^d$ ,  $f_1^u$ , and  $f_2^d$ ; for details see [2,6]. For the leading-twist distribution amplitude  $\varphi(x_i)$  we have also determined the next-to-next-to-leading conformal spin contributions which can be completely parametrized, e.g., by the moments  $\varphi^{101}$ ,  $\varphi^{200}$ , and  $\varphi^{002}$ . The local matrix elements defining the nonperturbative parameters up to next-to-leading conformal spin are (see [6] for the corrected formulas from [2])

$$\langle 0 | \epsilon^{ijk} [u^i C \not{x} u^j](0) [\gamma_5 \not{z} d^k]_{\delta}(0) | P \rangle = f_N (P \cdot z) \not{z} N_{\delta}(P), \quad (11)$$

$$\langle 0 | \varepsilon^{ijk} [u^i C \gamma_\mu u^j](0) [\gamma_5 \gamma^\mu d^k]_\delta(0) | P \rangle = \lambda_1 m_N N_\delta(P), \quad (12)$$

$$\langle 0 | \varepsilon^{ijk} [u^i C \sigma_{\mu\nu} u^j](0) [\gamma_5 \sigma^{\mu\nu} d^k]_\delta(0) | P \rangle = \lambda_2 m_N N_\delta(P), \quad (13)$$

$$\begin{aligned} \langle 0 | \varepsilon^{ijk} [u^i C \not{z} u^j](0) [\gamma_5 \not{z} i z \cdot \vec{D} d^k]_\delta(0) | P \rangle \\ = f_N V_1^d(P \cdot z)^2 \not{z} N_\delta(P), \end{aligned} \quad (14)$$

$$\begin{aligned} \langle 0 | \varepsilon^{ijk} [u^i C \not{z} \gamma_5 i z \cdot \vec{D} u^j](0) [\not{z} d^k]_\delta(0) | P \rangle \\ = -f_N A_1^u(P \cdot z)^2 \not{z} N_\delta(P), \end{aligned} \quad (15)$$

$$\begin{aligned} \langle 0 | \varepsilon^{ijk} [u^i C \gamma_\mu u^j](0) [\not{z} \gamma_5 \gamma^\mu i z \cdot \vec{D} d^k]_\delta(0) | P \rangle \\ = \lambda_1 f_1^d(P \cdot z) M \not{z} N_\delta(P), \end{aligned} \quad (16)$$

$$\begin{aligned} \langle 0 | \varepsilon^{ijk} [u^i C \sigma_{\mu\nu} u^j](0) [\not{z} \gamma_5 \sigma^{\mu\nu} i z \cdot \vec{D} d^k]_\delta(0) | P \rangle \\ = \lambda_2 f_2^d(P \cdot z) M \not{z} N_\delta(P), \end{aligned} \quad (17)$$

$$\begin{aligned} \langle 0 | \varepsilon^{ijk} [u^i C \gamma_\mu \gamma_5 i z \cdot \vec{D} u^j](0) [\not{z} \gamma^\mu d^k]_\delta(0) | P \rangle \\ = \lambda_1 f_1^u(P \cdot z) M \not{z} N_\delta(P), \end{aligned} \quad (18)$$

with the nucleon spinor  $N_\delta(P)$ , the nucleon mass  $m_N$ , an arbitrary lightlike vector  $z^\nu$  with  $z^2 = 0$  and  $\vec{D} = \vec{D} - \vec{D}$ . All derivatives act only on the quark fields and not on any explicit factor  $z$ . The second moments of the nucleon distribution amplitudes are related to the following local operators:

$$\begin{aligned} \langle 0 | \varepsilon^{ijk} [u^i C \not{z} u^j](0) [\gamma_5 \not{z} (i z \cdot \vec{D})^2 d^k]_\delta(0) | P \rangle \\ = f_N \varphi^{002}(P \cdot z)^3 \not{z} N_\delta(P), \end{aligned} \quad (19)$$

$$\begin{aligned} \langle 0 | \varepsilon^{ijk} [((i z \cdot \vec{D})^2 u^i) C \not{z} u^j](0) [\gamma_5 \not{z} d^k]_\delta(0) | P \rangle \\ - \langle 0 | \varepsilon^{ijk} [((i z \cdot \vec{D})^2 u^i) C \not{z} \gamma_5 u^j](0) [\not{z} d^k]_\delta(0) | P \rangle \\ = f_N \varphi^{200}(P \cdot z)^3 \not{z} N_\delta(P), \end{aligned} \quad (20)$$

$$\begin{aligned} \langle 0 | \varepsilon^{ijk} [(i z \cdot \vec{D} u^i) C \not{z} u^j](0) [\gamma_5 \not{z} i z \cdot \vec{D} d^k]_\delta(0) | P \rangle \\ - \langle 0 | \varepsilon^{ijk} [(i z \cdot \vec{D} u^i) C \not{z} \gamma_5 u^j](0) [\not{z} i z \cdot \vec{D} d^k]_\delta(0) | P \rangle \\ = f_N \varphi^{101}(P \cdot z)^3 \not{z} N_\delta(P). \end{aligned} \quad (21)$$

The parameters used in this work with their twist and conformal spin are summarized as follows:

	Leading twist	Higher twist
Leading conformal spin	$f_N$	$\lambda_1, \lambda_2$
Next-to-leading conformal spin	$A_1^u, V_1^d$	$f_1^u, f_1^d, f_2^d$
Next-to-next-to-leading conformal spin	$\varphi^{101}, \varphi^{200}, \varphi^{002}$	...

As in the meson case these parameters can be estimated with QCD sum rules [31] (see, e.g., [32–34] for some recent work in the meson case) or with lattice simulations (see, e.g., [35,36] for lattice works considering the same mesons).

### III. QCD SUM-RULE DETERMINATION OF THE NUCLEON DISTRIBUTION AMPLITUDES

The leading-twist distribution amplitude was investigated with QCD sum rules up to the second moments in [29,37] and up to the third moments in [30] including perturbative contributions and terms proportional to the gluon condensate and to the four-quark condensate (several errors in [29] were corrected in [30]).

The next-to-leading twist normalization constants  $\lambda_1$  and  $\lambda_2$  describe the coupling to the proton of two independent proton interpolating fields used in QCD sum rules,  $\lambda_1$  is the coupling of the so-called Ioffe current [38], while  $\lambda_2$  is the coupling of the interpolating nucleon field that was advocated in [39]. In [38,39] first QCD sum-rule estimates for  $\lambda_{1,2}$  were presented. Higher dimensional condensates were included in [40]. Unfortunately these pioneering works contain several misprints; for a review with the correct expressions see, e.g., [41,42].  $\alpha_s$  corrections were calculated by Jamin in [43]. They turned out to be very large ( $\approx +50\%$  for  $|\lambda_1^2|$ , corresponding to  $\approx +25\%$  for  $|\lambda_1|$ ), but we will not take them into account, since we also do not have  $\alpha_s$  corrections for the light-cone sum rules, connecting the distribution amplitudes with the nucleon form factors. In [6] contributions of nonplanar diagrams to the dimension 8 condensates were also included. Putting all this together (for the first time) the QCD sum-rule expression for  $\lambda_1$  reads

$$\begin{aligned} 2(2\pi)^4 m_N^2 |\lambda_1^2| = e^{m_N^2/M_B^2} \left\{ M_B^6 E_3 \right. \\ \times \left( \frac{s_0}{M_B^2} \right) L^{-4/9} \left( 1 + \left[ \frac{53}{12} + \gamma_E \right] \frac{\alpha_s(M_B^2)}{\pi} \right) \\ \left. + \frac{b}{4} M_B^2 E_1 \left( \frac{s_0}{M_B^2} \right) L^{-4/9} + \frac{a^2}{3} \left[ 4 - \frac{4}{3} \frac{m_0^2}{M_B^2} \right] \right\}, \end{aligned} \quad (22)$$

where  $M_B$  is the Borel parameter,  $s_0$  is the continuum threshold, and

$$E_n(s_0/M^2) = 1 - e^{-(s_0/M^2)} \sum_{k=0}^{n-1} \frac{1}{k!} \left( \frac{s_0}{M^2} \right)^k, \quad (23)$$

$$L = \frac{\alpha_s(\mu^2)}{\alpha_s(M_B^2)}, \quad (24)$$

$$a = -(2\pi)^2 \langle \bar{q}q \rangle \simeq 0.55 \text{ GeV}^3, \quad (25)$$

$$b = (2\pi)^2 \left\langle \frac{\alpha_s}{\pi} G^2 \right\rangle \simeq 0.47 \text{ GeV}^4, \quad (26)$$

$$m_0^2 = \frac{\langle \bar{q}gGq \rangle}{\langle \bar{q}q \rangle} \simeq 0.65 \text{ GeV}^2. \quad (27)$$

We have neglected in Eq. (22) the small  $\alpha_s$  corrections to the four-quark contribution proportional to  $a^2$ . The corresponding formula for  $\lambda_2$  can be found, e.g., in [6]. QCD sum-rule estimates for the  $f_N^v$  defined in Eqs. (16)–(18) were first presented in [2] and updated in [6]. The parameter set which is obtained by QCD sum rules will be called the *sum-rule* estimate in the following; we use the numerical values from [30] for the moments of the leading-twist distribution amplitude and the values from [6] for  $f_N$ ,  $\lambda_1$ ,  $\lambda_2$ ,  $A_1^u$ ,  $V_1^d$ ,  $f_1^d$ ,  $f_1^u$ , and  $f_2^d$ . In our analysis we use two related parameter sets which are based on the QCD sum-rule determination:

- (i) Demanding that all higher conformal contributions vanish, fixes  $A_1^u$ ,  $V_1^d$ ,  $f_1^d$ ,  $f_1^u$ , and  $f_2^d$ , while the values for  $f_N$ ,  $\lambda_1$ , and  $\lambda_2$  are taken from the QCD sum-rule estimates or from the lattice calculation. This parameter set will be called *asymptotic*. In the case of the leading twist, one would be left with the asymptotic distribution amplitude  $\varphi(x_i, Q^2 \rightarrow \infty) = \varphi_{\text{asy}}(x_i) = 120x_1x_2x_3f_N$ . The corresponding expressions for the higher twist distribution amplitudes can be found in [2].
- (ii) With the help of light-cone sum rules [6,16,44] one can express the nucleon form factors in terms of the eight nonperturbative parameters  $f_N$ ,  $\lambda_1$ ,  $\lambda_2$ ,  $A_1^u$ ,  $V_1^d$ ,  $f_1^d$ ,  $f_1^u$ , and  $f_2^d$  (including twist-6 corrections and expanding the distribution amplitudes up to the next-to-leading conformal spin). Choosing values for these parameters in between the asymptotic and the sum-rule values, we got an astonishingly good agreement with the experimental numbers; see [6]. This procedure is obviously rather *ad hoc* and has to be replaced by a real fit after  $\alpha_s$  corrections to the light-cone sum rules have been calculated. The parameter set obtained in [6] will be called BLW.

#### IV. LATTICE DETERMINATION OF THE NUCLEON DISTRIBUTION AMPLITUDES

Lattice QCD offers the possibility to perform nonperturbative computations in QCD without additional model assumptions. For example, one can evaluate hadron masses and matrix elements of local operators between hadron states. In particular, the nonperturbative parameters  $f_N, \dots$  introduced above can be extracted from Monte Carlo simulations on the lattice as advocated in [45].

Recently, the QCDSF Collaboration performed such a calculation [4]. It is based on gauge field configurations generated with two dynamical flavors of quarks. For the

gauge field the standard Wilson action was used, while the lattice action for the quarks was the so-called nonperturbatively  $O(a)$  improved Wilson fermion action, also known as the clover fermion action. Although lattice artifacts seem to be small, a reliable continuum extrapolation could not be attempted, and we utilize here the data obtained on the finest lattice corresponding to a gauge coupling parameter  $\beta = 5.40$ . Setting the scale via a Sommer parameter of  $r_0 = 0.467$  fm the lattice spacing turns out to be  $a \approx 0.067$  fm.

On the lattice, matrix elements between the vacuum and a nucleon such as those needed here are computed from two-point correlation functions of the local operator  $\mathcal{O}_\alpha(x)$  under study and a suitable interpolating field  $\tilde{\mathcal{N}}_\alpha(x)$  for the nucleon.

Asymptotically this two-point function decays exponentially with the distance between the operators since the lattice calculations are performed in Euclidean space. Projecting onto definite momentum one finds for sufficiently large (Euclidean) times  $t$ :

$$\begin{aligned} & \sum_{\vec{x}} \sum_{\vec{y}} e^{-i\vec{P}\cdot\vec{x}} e^{i\vec{P}\cdot\vec{y}} \langle \mathcal{O}_\alpha(\vec{x}, t) \tilde{\mathcal{N}}_\beta(\vec{y}, 0) \rangle \\ &= \frac{V_s \sqrt{Z}}{2E(\vec{P})} M_{\mathcal{O}}(E(\vec{P})) \gamma_4 - i\vec{P} \cdot \vec{\gamma} + m_N)_{\alpha\beta} e^{-E(\vec{P})t}. \end{aligned} \quad (28)$$

Here  $V_s$  denotes the spatial volume of the lattice and the matrix elements of  $\mathcal{O}_\alpha(x)$  and  $\tilde{\mathcal{N}}_\alpha(x)$  have been represented as

$$\langle 0 | \mathcal{O}_\alpha(0) | P \rangle = M_{\mathcal{O}} N_\alpha(P), \quad (29)$$

$$\langle P | \tilde{\mathcal{N}}_\alpha(0) | 0 \rangle = \sqrt{Z} \tilde{N}_\alpha(P). \quad (30)$$

As the local operators  $\mathcal{O}_\alpha(x)$  used in the simulations are linear combinations of the operators appearing in (11)–(21), the constants  $M_{\mathcal{O}}$  are directly related to moments of the distribution amplitudes.

The operators  $\mathcal{O}_\alpha(x)$  need to be renormalized. In Ref. [4] a nonperturbative renormalization procedure has been chosen. As the space-time symmetry on the lattice is reduced to the finite (spinorial) hypercubic group, the mixing pattern of our three-quark operators is more complicated than in the continuum and the choice of the operators becomes an important issue. Guided by the group-theoretical classification of three-quark operators given in [46] the problematic mixing with lower dimensional operators could however be completely avoided. Moreover, the freedom in the choice of the operators has been exploited in order to reduce the statistical uncertainties of the results.

Primarily, the combination of moments

$$\begin{aligned} \varphi^{n_1 n_2 n_3} &= \frac{1}{3} (V_1^{n_1 n_2 n_3} - A_1^{n_1 n_2 n_3} + 2T_1^{n_1 n_3 n_2}) \\ &= \frac{1}{3} (2\varphi^{n_1 n_2 n_3} + \varphi^{n_3 n_2 n_1}) \end{aligned} \quad (31)$$

has been evaluated, from which the combination  $\varphi^{n_1 n_2 n_3}$  usually used in sum-rule calculations is readily obtained by

$$\varphi^{n_1 n_2 n_3} = 2\phi^{n_1 n_2 n_3} - \phi^{n_3 n_2 n_1}. \quad (32)$$

In the following sections we shall compare these lattice results with results obtained from other approaches and see what the lattice numbers imply for the nucleon form factors.

## V. COMPARISON OF DIFFERENT METHODS TO DETERMINE THE DISTRIBUTION AMPLITUDES

In Table I we compare different estimates for the moments of the leading-twist distribution amplitude at 1 GeV<sup>2</sup>. It turns out that the BLW model, the Bolz-Kroll (BK) model, and the lattice evaluation give almost identical results, which are close to the asymptotic values, while the QCD sum-rule estimates seem to overestimate the deviation from the asymptotic form, although the deviation goes in the right direction. The BLW model was inspired by this experience: One starts with the asymptotic form and

goes then in the direction of the QCD sum-rule estimate, but only for a fraction of the whole difference. Choosing this fraction to be 1/3 one gets an astonishingly good agreement between light-cone sum-rule predictions for the nucleon form factors and experiment; see [6]. In the same spirit one can make a BLW model for the second moments, also given in Table I [48]. These values are again very close to the lattice values. The BK model [47] was also inspired by experiment, in particular, the decay  $J/\Psi \rightarrow N\bar{N}$ , the Feynman contribution to the nucleon form factor, and the valence quark distribution function.

In Table II we compare different estimates for  $f_N$ ,  $\lambda_1$ ,  $\lambda_2$ ,  $A_1^u$ ,  $V_1^d$ ,  $f_1^d$ ,  $f_1^u$ , and  $f_2^d$  at 1 GeV<sup>2</sup>. The leading-twist parameters  $A_1^u$  and  $V_1^d$  are already fully contained in Table I via the relations

$$A_1^u = 2\varphi^{100} + \varphi^{001} - 1, \quad (33)$$

$$V_1^d = \varphi^{001}. \quad (34)$$

Let us stress, however, that the errors quoted in Tables I and II have to be taken with caution. On the lattice side a

TABLE I. Comparison of different estimates for the moments of the leading-twist distribution amplitude renormalized at 1 GeV<sup>2</sup>. We show the asymptotic values (Asy) and the QCD sum-rule estimates from [30]. Inspired by the QCD sum-rule calculation two models for the leading-twist distribution amplitude were suggested, the COZ model [30] and the KS model [37]. Using also some experimental input two phenomenological models were introduced, the BK model [47] and the BLW model [6]. Finally we show the lattice values from [3–5]. The first error is statistical, and the second error represents the uncertainty due to the chiral extrapolation and renormalization. For the BK model no contributions from next-to-next-to-leading conformal spin were taken into account; thus the second moments denoted by the  $\star$  do not contain any additional information and are fully determined by the first moments.

	Asy.	QCD-SR	COZ	KS	BK	BLW	LAT
$\varphi^{100}$	$\frac{1}{3} \approx 0.333$	0.560(60)	0.579	0.55	$\frac{8}{21} \approx 0.38$	0.415	0.3999(37)(139)
$\varphi^{010}$	$\frac{1}{3} \approx 0.333$	0.192(12)	0.192	0.21	$\frac{13}{42} \approx 0.31$	0.285	0.2986(11)(52)
$\varphi^{001}$	$\frac{1}{3} \approx 0.333$	0.229(29)	0.229	0.24	$\frac{13}{42} \approx 0.31$	0.300	0.3015(32)(106)
$\varphi^{200}$	$\frac{1}{7} \approx 0.143$	0.350(70)	0.369	0.35	$\frac{5}{28} \approx 0.18^\star$	0.225	0.1816(64)(212)
$\varphi^{020}$	$\frac{1}{7} \approx 0.143$	0.084(19)	0.068	0.09	$\frac{1}{8} \approx 0.13^\star$	0.121	0.1281(32)(106)
$\varphi^{002}$	$\frac{1}{7} \approx 0.143$	0.109(19)	0.089	0.12	$\frac{1}{8} \approx 0.13^\star$	0.132	0.1311(113)(382)
$\varphi^{011}$	$\frac{2}{21} \approx 0.095$	-0.030(30)	0.027	0.02	$\frac{1}{12} \approx 0.08^\star$	0.071	0.0613(89)(319)
$\varphi^{101}$	$\frac{2}{21} \approx 0.095$	0.102(12)	0.113	0.10	$\frac{17}{168} \approx 0.10^\star$	0.097	0.1091(41)(152)
$\varphi^{110}$	$\frac{2}{21} \approx 0.095$	0.090(10)	0.097	0.10	$\frac{8}{21} \approx 0.10^\star$	0.093	0.1092(67)(219)

TABLE II. Comparison of different estimates for  $f_N$ ,  $\lambda_1$ ,  $\lambda_2$ ,  $A_1^u$ ,  $V_1^d$ ,  $f_1^d$ ,  $f_1^u$ , and  $f_2^d$  renormalized at 1 GeV<sup>2</sup>. The QCD sum-rule estimates and the BLW values are taken from [6] and we also show the phenomenological model from [47] (BK). For the asymptotic and the BLW parameters the values for  $f_N$ ,  $\lambda_1$ , and  $\lambda_2$  coincide with the ones from the QCD sum-rule estimates.

	Asy.	QCD-SR	BK	BLW	LAT
$f_N \times 10^3$ (GeV <sup>2</sup> )	5.0(5)	5.0(5)	6.64	5.0(5)	3.234(63)(86)
$\lambda_1 \times 10^3$ (GeV <sup>2</sup> )	-27(9)	-27(9)	...	-27(9)	-35.57(65)(136)
$\lambda_2 \times 10^3$ (GeV <sup>2</sup> )	54(19)	54(19)	...	54(19)	70.02(128)(268)
$A_1^u$	0	0.38(15)	$\frac{1}{14} \approx 0.071$	0.13	0.1013(81)(298)
$V_1^d$	$\frac{1}{3} \approx 0.333$	0.23(3)	$\frac{13}{42} \approx 0.31$	0.30	0.3015(32)(106)
$f_1^d$	0.30	0.40(5)	...	0.33	...
$f_1^u$	0.10	0.07(5)	...	0.09	...
$f_2^d$	$\frac{4}{15} \approx 0.267$	0.22(5)	...	0.25	...

continuum extrapolation could not be attempted, and hence the associated systematic error is not included. Moreover, the errors on  $A_1^u$  have been calculated by error propagation, which might not be too reliable. For the sum-rule estimates the radiative corrections are expected to be sizable, but these are only known for  $\lambda_1$  and  $\lambda_2$ . The central lattice value of  $f_N$  is about 35% smaller than the QCD sum-rule estimates, while the lattice results for  $|\lambda_1|$  and  $|\lambda_2|$  are about 30% larger than the QCD sum-rule estimates. For  $\lambda_1$  and  $\lambda_2$  the discrepancy is strongly reduced, if radiative corrections to the sum-rule estimates are included, cf. Equation (22), for  $f_N$ —according to our knowledge—no radiative corrections have been calculated yet.

The parameters  $\lambda_1$  and  $\lambda_2$  can also be extracted from the lattice calculation of the nucleon decay matrix elements (expressed in terms of the parameters  $\alpha$  and  $\beta$ ) in [25,26]. Using the relations

$$\lambda_1 = \frac{4}{m_N} \alpha, \quad \lambda_2 = \frac{8}{m_N} \beta, \quad (35)$$

we obtain from the results in [25,26]

$$\lambda_1 = -43.90 \pm 4.7 \pm 8.5 \times 10^{-3} \text{ GeV}^2, \\ \lambda_2 = 93.96 \pm 10.2 \pm 22.7 \times 10^{-3} \text{ GeV}^2,$$

at the renormalization scale  $1 \text{ GeV}^2$ . In that case the deviation from the QCD sum-rule values is even more pronounced.

In the nonrelativistic limit one gets

$$2\lambda_1 + \lambda_2 = 0.$$

The estimates presented in Table II fulfill this relation almost perfectly:

$$\left. \frac{2\lambda_1 + \lambda_2}{2\lambda_1 - \lambda_2} \right|_{\text{QCD-SR}} = 0 \pm 0.24, \quad (36)$$

$$\left. \frac{2\lambda_1 + \lambda_2}{2\lambda_1 - \lambda_2} \right|_{\text{LAT}} = 0.008 \pm 0.013. \quad (37)$$

For the ratio  $f_N/\lambda_1$  the differences between the central lattice and QCD sum-rule estimates are even more enhanced:

$$\left. \frac{f_N}{\lambda_1} \right|_{\text{QCD-SR}} = -0.185 \pm 0.064, \quad (38)$$

$$\left. \frac{f_N}{\lambda_1} \right|_{\text{LAT}} = -0.0909 \pm 0.0054 \pm 0.0095. \quad (39)$$

The QCD sum-rule estimate is a factor of 2 larger than the lattice result. In the next section we will see that the electromagnetic form factors of the nucleon depend only on the ratio but not on the individual values of  $f_N$  and  $\lambda_1$ , if the so-called Ioffe interpolating field is used, while the  $N \rightarrow \Delta$  transition depends on the individual values.

## VI. LIGHT-CONE SUM RULES FOR FORM FACTORS

LCSRs are an advancement of QCD sum rules [31] for intermediate values of the momentum transfer  $Q^2$ , i.e.,  $1 \text{ GeV}^2 < Q^2 < 10 \text{ GeV}^2$  in the case of nucleon form factors. They were introduced in [17,18]. The starting point is a correlation function of the form

$$T(P, q) = \int d^4x e^{-iqx} \langle 0 | T \{ \eta(0) j(x) \} | N(P) \rangle, \quad (40)$$

which describes the transition of a baryon  $B$  with momentum  $P - q$  to the nucleon  $N(P)$  via the current  $j$ . The baryon  $B$  is created by the interpolating three-quark field  $\eta$ . If  $B$  is a nucleon one can use, e.g., the Ioffe current [38] for the proton

$$\eta_{\text{Ioffe}}(x) = \epsilon^{ijk} [u^i(x) (C \gamma_\nu) u^j(x)] (\gamma_5 \gamma^\nu) d_\delta^k(x). \quad (41)$$

A typical example for  $j$  is the electromagnetic current in the case of the electromagnetic form factors

$$j_\mu^{\text{EM}}(x) = e_u \bar{u}(x) \gamma_\mu u(x) + e_d \bar{d}(x) \gamma_\mu d(x). \quad (42)$$

With the definitions in Eqs. (41) and (42) the correlation function in Eq. (40) describes the electromagnetic form factors of the nucleon, which can be measured, e.g., in elastic electron-proton scattering.

The basic idea of the light-cone sum-rule approach is to calculate the correlation function in Eq. (40) both on the hadron level (expressed in terms of form factors) and on the quark level (expressed in terms of the nucleon distribution amplitudes). Equating both results and performing a Borel transformation to suppress higher mass states one can express the form factors in terms of the eight (taking only leading and next-to-leading conformal spin into account) nonperturbative parameters of the nucleon distribution amplitudes, the Borel parameter  $M_B$ , and the continuum threshold  $s_0$ ; for details see [6,16].

We studied the electromagnetic nucleon form factors with the Chernyak-Zhitnitsky interpolating field ( $\eta_{\text{CZ}}$ ) in [16]. In [44] we found that  $\eta_{\text{CZ}}$  yields large unphysical isospin violating effects; therefore we introduced a new isospin respecting CZ-like current to determine the electromagnetic form factors. In [6] we also studied the Ioffe current for the nucleon and extended our studies from the electromagnetic form factors to axial form factors, pseudoscalar form factors, and the neutron to proton transition. It turned out that the Ioffe current yields the most reliable results. Despite our “bad experience”  $\eta_{\text{CZ}}$  was used to determine the scalar form factor of the nucleon [49] and the axial and the pseudoscalar one in [50]. The question of the ideal interpolating field can also be addressed more generally: One can write down the most general interpolating field—without derivatives—of the nucleon as a linear combination of two currents and then try to optimize the relative strength of these currents. This approach was used for the scalar form factor of the nucleon in [51], for the

axial-vector form factors in [52], and for the electromagnetic form factors in [53]. Since in [53]  $x^2$  corrections were not included and different Dirac projections to extract the sum rules were used, we cannot easily compare the result with [6].

The light-cone sum-rule method can also be applied to other observables than the nucleon form factors.

In the class of nucleon to resonance transitions the following processes were considered: The  $N \rightarrow \Delta$  transition was studied in this framework in [54] (for a similar approach for  $Q^2 = 0$  see, e.g., [55]), and the axial part of the  $N \rightarrow \Delta$  transition was calculated in [56]. Very recently the form factors of the  $N \rightarrow N^*(1535)$  transition were presented in [57]. In [58–60] pion electroproduction was investigated.

Also decays of baryons can be described with that formalism:  $\Lambda_b \rightarrow p l \nu$  was discussed in [27]. The authors of [61] considered  $\Lambda_c \rightarrow \Lambda l \nu$  and therefore determined a part of the  $\Lambda$  distribution amplitude. In [62] the transition  $\Sigma \rightarrow N$  was investigated. Recently the rare decays  $\Lambda_b \rightarrow \Lambda \gamma$  and  $\Lambda_b \rightarrow \Lambda l^+ l^-$  were treated in [63] with the same formalism. Electromagnetic form factors of  $\Sigma$  and  $\Lambda$  baryons were estimated in [64,65].

So far all mentioned LCSR calculations for the baryon form factors were done in leading-order QCD. One expects sizable radiative corrections of up to 30%. In [66] a first step in calculating the full  $\mathcal{O}(\alpha_s)$  corrections to the nucleon electromagnetic form factors was performed. The intrinsic final uncertainty of this approach is expected to be in the range of less than  $\pm 20\%$ , if QCD corrections are included. Comparing the theoretical predictions with experimental numbers one must be careful to distinguish between quantities directly calculated like  $F_1$  and  $F_2$  and quantities like  $G_E = F_1 - Q^2/(4m_N^2)F_2$  for which cancellations might ruin the predictive power.

In the following we use the LO QCD light-cone sum rules of [6] for the electromagnetic form factors of the nucleon and the LO QCD results of [54] for the  $N \rightarrow \Delta$  transition to compare the consequences for the form factors which the lattice results for the nucleon distribution amplitudes entail with those which result from different QCD sum-rule estimates. Note, however, that the errors on the nonperturbative parameters of the nucleon distribution amplitudes will not be taken into account, because this would not make much sense due to the inherent uncertainty in the LO light-cone sum rules.

## VII. RESULTS FOR THE FORM FACTORS AT INTERMEDIATE MOMENTUM TRANSFER

In this section we use light-cone sum rules to extract physical form factors from the nucleon distribution amplitudes, by taking into account conformal spin contributions up to the  $p$ -wave;  $d$ -wave effects will be discussed in Sec. IX.

We compare our theory results to the following experimental numbers. For the electromagnetic nucleon form factors we take data from the following:

- (i) The magnetic form factor of the proton normalized to the dipole form factor  $G_M^p/(\mu_p G_D)$  from [67–75], with

$$G_D(Q^2) = \frac{1}{(1 + \frac{Q^2}{0.71 \text{ GeV}^2})^2}, \quad \mu_p = 2.7928 \dots \quad (43)$$

The data of [69–71] are actually taken from the reanalysis in [76].

- (ii) The ratio of the electric and magnetic form factors of the proton  $\mu_p G_E^p/G_M^p$  from Rosenbluth separation [67–75,77–79] and from polarization transfer [19–22]. We would like to point out here that [74,75] claimed already in the 1970s a steeper  $Q^2$  dependence of  $G_E^p$  compared to  $G_M^p$  for momentum transfers above  $1 \text{ GeV}^2$ . Currently the Rosenbluth separation data for  $G_E$  are judged to be less reliable.
- (iii) The ratio of the proton form factors  $F_1^p$  and  $F_2^p$  given as  $\sqrt{Q^2} F_1^p / ((\mu_p - 1) F_2^p)$  in [67,68,80].
- (iv) The magnetic form factor of the neutron normalized to the dipole form factor:  $G_M^n/(\mu_n G_D)$  from [74,81–87] with  $\mu_n = -1.913 \dots$ .
- (v) The electric form factor of the neutron normalized to the dipole form factor:  $G_E^n/G_D$  from [74,81,84,88–101]. The data are very well described by the so-called Galster fit [102]; we show in our plots the update of the Galster fit from Kelly [103]:

$$G_E^{n,\text{Galster}}(Q^2) = \frac{(1.70 \pm 0.04)\tau}{1 + (3.30 \pm 0.32)\tau} G_D(Q^2),$$

$$\text{with } \tau = \frac{Q^2}{4m_p^2}. \quad (44)$$

For the axial form factors we compare our result to the dipole formula [104]

$$G_A(Q^2) = \frac{1.267}{(1 + \frac{Q^2}{(1.014 \text{ GeV})^2})^2}. \quad (45)$$

For more details see [6].

Finally we use the following data for the  $N \rightarrow \Delta$  transition:

- (i) The magnetic form factor normalized to the dipole form factor  $G_M^*/(3G_D)$  from [105–112].
- (ii) The ratio of the electric quadrupole to the magnetic form factor  $R_{EM}$  from [112,113].
- (iii) The ratio of the Coulomb quadrupole to the magnetic form factor  $R_{SM}$  from [112,113].

For more details see [54]. Since we compare the data with the LCSR predictions, which are expected to work best in the region  $1 \text{ GeV}^2 < Q^2 < 10 \text{ GeV}^2$ , we are only

interested in experiments where values of the form factors for momentum transfer above  $Q^2 = 1 \text{ GeV}^2$  are available.

For the theory prediction we will use six models (i.e., six determinations for the nonperturbative parameters  $f_N$ ,  $\lambda_1$ ,  $\lambda_2$ ,  $A_1^u$ ,  $V_1^d$ ,  $f_1^d$ ,  $f_1^u$ , and  $f_2^d$ ) for the nucleon distribution amplitudes including  $s$ - and  $p$ -wave contributions:

- (1) QCD sum-rule estimates (dotted red lines in Figs. 1–5),
- (2) asymptotic form (dashed red lines),
- (3) BLW model (solid red lines),
- (4) lattice evaluation plus QCD sum-rule estimate for  $f_x^y$  (dotted blue lines),
- (5) lattice evaluation plus asymptotic values for  $f_x^y$  (dashed blue lines),
- (6) lattice evaluation plus BLW estimate for  $f_x^y$  (solid blue lines).

Since  $f_1^d$ ,  $f_1^u$ , and  $f_2^d$  have not been determined on the lattice, we have to use in the lattice parameter set QCD sum-rule estimates, asymptotic values, or the BLW model for  $f_x^y$ . For the nucleon form factors we use the LCSRs obtained in [6] and for the  $N \rightarrow \Delta$  transition we use the LCSRs obtained in [54].

To our accuracy, the sum rules for the nucleon form factors depend only on the five parameters  $f_N/\lambda_1$ ,  $A_1^u$ ,  $V_1^d$ ,  $f_1^u$ , and  $f_1^d$ . Within the light-cone sum-rule approach we determine the form factors  $F_1$  and  $F_2$  directly. The electric

and the magnetic form factors  $G_E$  and  $G_M$  are linear combinations of  $F_1$  and  $F_2$ :

$$\begin{aligned} G_M(Q^2) &= F_1(Q^2) + F_2(Q^2), \\ G_E(Q^2) &= F_1(Q^2) - \frac{Q^2}{4m_N^2} F_2(Q^2). \end{aligned} \quad (46)$$

As discussed above, Eq. (46) shows that in  $G_E$  cancellations occur. Therefore our predictions for  $G_E$  are less reliable than those for  $G_M$ .

The light-cone sum-rule predictions for the form factors are shown in Figs. 1–4. For  $G_M^p$ ,  $G_A^p$ ,  $G_M^n$ , and  $G_E^n$  the differences between the lattice determinations and the other approaches (asymptotic, QCD sum rule, and BLW) are smaller than the expected overall uncertainties, i.e., the pairs of parameter sets (1)–(4), (2)–(5), and (3)–(6) yield almost identical results. Since  $f_1^u$  and  $f_1^d$  were chosen to be identical within these pairs, differences can only occur due to  $V_1^d$ ,  $A_1^u$ , and  $f_N/\lambda_1$ . The lattice values for  $V_1^d$  and  $A_1^u$  are very close to the BLW values, while  $f_N/\lambda_1$  is in the lattice determination about a factor of 2 smaller than the QCD sum-rule estimate. In  $G_E$ ,  $\sqrt{Q^2} F_2^p / ((\mu_p - 1) F_1^p)$  and  $G_T^p$  cancellations occur, so we expect much bigger theoretical uncertainties and also big differences between our data sets might be possible.

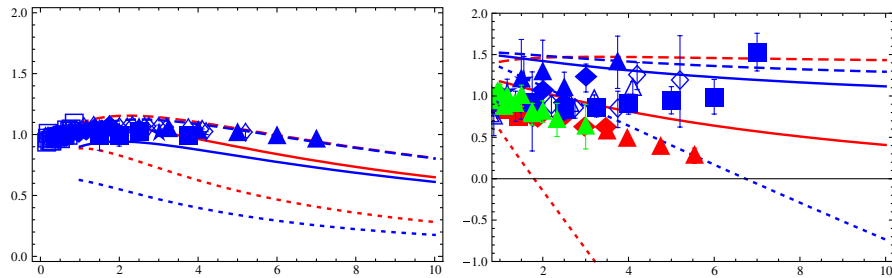


FIG. 1 (color online). LCSR results for the electromagnetic form factors (left panel:  $G_M/(\mu_p G_D)$  vs  $Q^2$ ; right panel:  $\mu_p G_E/G_M$  vs  $Q^2$ ) of the proton. In the left panel the curves correspond to the models (2), (5), (3), (6), (1), and (4) (from top to bottom), where (2) and (5) are almost identical. In the right panel the curves correspond to the models (2), (5), (6), (3), (4), and (1) (from top to bottom on the right). The gray (red) triangles in the right panel are JLAB data, while the dark gray (blue) data points and the light gray (green) triangles are obtained via Rosenbluth separation. Currently the Rosenbluth separation data for  $G_E$  are judged to be less reliable.

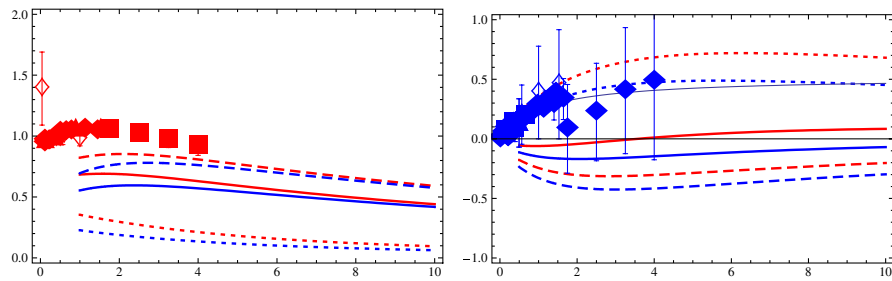


FIG. 2 (color online). LCSR results for the electromagnetic form factors of the neutron (left panel:  $G_M/(\mu_n G_D)$  vs  $Q^2$ ; right panel:  $G_E/(G_D)$  vs  $Q^2$ ). In the left panel the curves correspond to the models (2), (5), (3), (6), (1), and (4) (from top to bottom). In the right panel the thick curves correspond to the models (1), (4), (3), (6), (2), and (5) (from top to bottom), while the thin solid (blue) line represents the updated Galster fit.

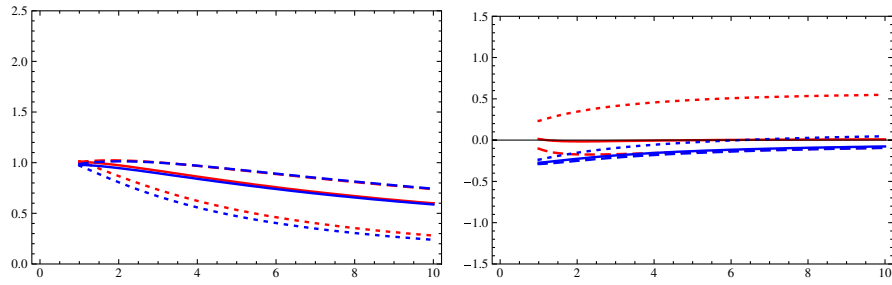


FIG. 3 (color online). LCSR results for the axial form factor of the proton  $G_A$  normalized to  $G_D = g_A/(1 + Q^2/m_A^2)^2$  vs  $Q^2$  (left panel) and the tensor form factor  $G_T$  normalized to  $G_A$  vs  $Q^2$  (right panel). In the left panel the curves correspond to the models (2), (5), (3), (6), (1), and (4) (from top to bottom), where (2) and (5) as well as (3) and (6) are almost identical. In the right panel the curves correspond to the models (1), (3), (2), (4), (6), and (5) (from top to bottom on the left), where (3) yields nearly zero.

The data for  $G_M^p$  (Fig. 1) are very well described with the asymptotic and the BLW data sets, the differences between the parameter sets (2) and (5) and between (3) and (6) are negligible. The pure QCD sum-rule estimates [sets (1) and (4)] are about a factor of 2 too small. In the case of  $G_M^n$  (Fig. 2) one sees the same structure for the different models of the nucleon distribution amplitude as for  $G_M^p$ , but now all theory predictions are shifted to lower values. For  $G_A^p$  (Fig. 3) we agree for  $Q^2$  values below 5  $\text{GeV}^2$  very well with the dipole behavior, if we use the asymptotic or the BLW parameters; for higher  $Q^2$  we predict a slightly steeper falloff. Again the pure QCD sum-rule estimates are considerably worse. An interesting test of our approach is whether the unphysical tensor form factor  $G_T$  (Fig. 3) is consistent with zero. This holds for all parameter sets except the pure QCD sum-rule estimates [set (1)]. In our approach  $G_T^p$  is not exactly zero, because we treat the initial proton state differently from the final proton state: one is described by an interpolating nucleon field, the other by the nucleon distribution amplitude.

Finally we have the ratios  $G_E^n/G_D$  (Fig. 2),  $G_E^p/G_M^p$  (Fig. 1), and  $\sqrt{Q^2}F_2^p/((\mu_p - 1)F_1^p)$  (Fig. 4), which are very sensitive to the explicit form of the nucleon distribution amplitudes due to cancellations in  $G_E$ . If we just look

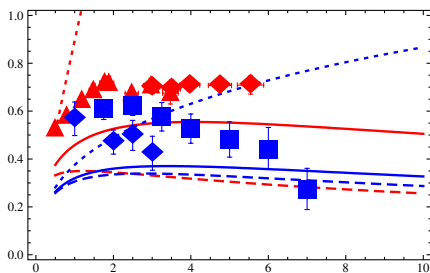


FIG. 4 (color online). LCSR results for the ratio  $\sqrt{Q^2}F_2^p/(F_1^p * 1.79)$ . The curves correspond to the models (1), (4), (3), (6), (5), and (2) (from top to bottom on the right). Gray (red) symbols: experimental values obtained via polarization transfer. Dark gray (blue) symbols: experimental values obtained via Rosenbluth separation. Currently the Rosenbluth separation data for  $G_E$  are judged to be less reliable.

at  $G_E^n$  our result would be consistent with zero and therefore describes the data well. If we investigate  $G_E^n/G_D$ , we blow up the large  $Q^2$  contributions. Now we have a “perfect” agreement between the pure QCD sum-rule parameters and the data. Our data set (4) is almost identical to the updated Galster fit. The BLW model is consistent with zero, while the asymptotic distribution amplitude yields negative values. The difference between the lattice values for the distribution amplitudes and the data sets (1)–(3) is visible, but not dramatic. In the case of  $G_E^p/G_M^p$  and  $\sqrt{Q^2}F_2^p/(F_1^p * 1.79)$  we can make similar observations. The purely asymptotic values lie above (below) the data for  $G_E^p/G_M^p$  [ $\sqrt{Q^2}F_2^p/(F_1^p * 1.79)$ ], the BLW data set moves the results in the right direction, but not far enough. Our data set (1) is completely off, because it predicts a very small value for  $F_1^p$ . Now we also have big differences between the lattice values of the distribution amplitudes and the pure QCD sum-rule values.

Taking into account that the full  $\mathcal{O}(\alpha_s)$  corrections to the LCSRs are not yet available, already a rough agreement of our approach with the data is a success. For  $G_M^p$ ,  $G_A^p$ ,  $G_M^n$ , and  $G_E^n$  we get unexpectedly “good” results if we use the BLW form or the asymptotic form of the nucleon distribution amplitude. The corresponding lattice values [sets (5) and (6)] give similar results. For  $G_E^n/G_D$ ,  $G_E^p/G_M^p$ , and  $\sqrt{Q^2}F_2^p/(F_1^p * 1.79)$  the BLW model lies in the right ball park, but we would prefer a model for the distribution amplitudes which lies in the middle between the asymptotic and the pure QCD sum-rule estimate (BLW is closer to the asymptotic value).

In the transition form factors of  $\gamma^*N \rightarrow \Delta$  all eight nonperturbative parameters appear; see [54]. The results are shown in Fig. 5. As expected, now the differences between the parameter set pairs (1)–(4), (2)–(5), and (3)–(6) are more pronounced. In the case of  $G_M^*$  the theory curves generally tend to be more flat than the experimental data. The form factors obtained with the lattice values for the nucleon distribution amplitude lie considerably above the data sets (1)–(3). Above  $Q^2 \approx 3 \text{ GeV}^2$  the asymptotic distribution amplitude and the BLW distribution amplitude

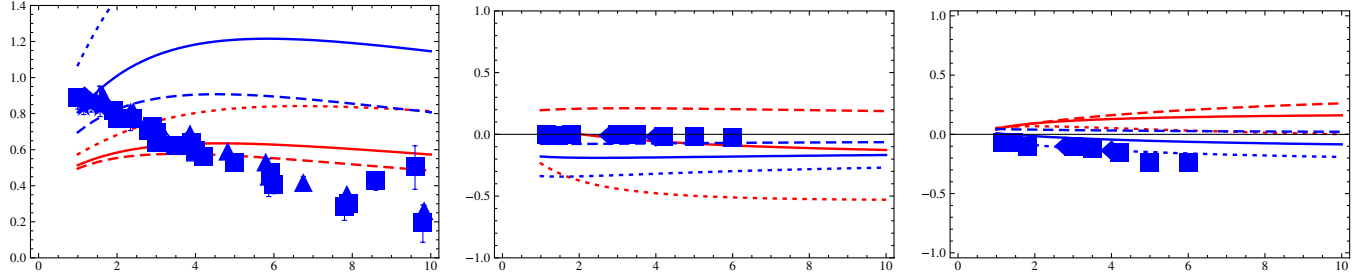


FIG. 5 (color online).  $\gamma^*N \rightarrow \Delta$  transition form factors [left panel:  $G_M^*/(3G_D)$  vs  $Q^2$ ; middle panel:  $R_{EM}$  vs  $Q^2$ ; right panel:  $R_{SM}$  vs  $Q^2$ ] in the LCSR approach [54]. In the left panel the curves correspond to the models (4), (6), (5), (1), (3), and (2) (from top to bottom on the left). In the middle panel the curves correspond to the models (2), (5), (3), (6), (4), and (1) (from top to bottom on the right). In the right panel the curves correspond to the models (2), (3), (5), (1), (6), and (4) (from top to bottom on the right), where (5) and (1) are almost identical.

are close to the data. The fact that  $R_{EM}$  is close to zero is reproduced very well with the BLW parameters [sets (3) and (6)] and the lattice plus asymptotic values [set (5)], while positive values are obtained with the purely asymptotic form [set (2)]. One gets a negative result with the QCD sum-rule determination of the nucleon distribution amplitude [sets (1) and (4)]. In the case of  $R_{SM}$  the differences are not very pronounced; all values are close to zero. Altogether one has to conclude that while all approaches give the correct order of magnitude none gives a really convincing description of all data. However in view of the fact that the systematic uncertainties are even more pronounced than for the nucleon form factors more could not have been expected.

### VIII. REDUCING THE NUMBER OF INDEPENDENT PARAMETERS OF THE DISTRIBUTION AMPLITUDES

In [114] the following approximate relations between twist-4 and twist-3 parameters were derived:

$$f_1^d = \frac{3}{10} - \frac{1}{6} \frac{f_N}{\lambda_1}, \quad f_1^u = \frac{1}{10} - \frac{1}{6} \frac{f_N}{\lambda_1}. \quad (47)$$

Using these relations, we can express the nucleon form factors in terms of only three independent parameters,

namely,  $\frac{f_N}{\lambda_1}$ ,  $V_1^d$ , and  $A_1^u$ . For the comparison with the data in Figs. 6–10 we show now only two models for the remaining three parameters of the nucleon distribution amplitude: (a) lattice determination of the distribution amplitude—blue curve and (b) BLW model—red curve.

We obtain the following values for  $f_1^x$ :

	(a)	(b)	Asymptotic	BLW	QCD-SR
$f_1^u$	0.11	0.13	0.10	0.09	0.07
$f_1^d$	0.31	0.33	0.30	0.33	0.40

which are compared with our previous estimates for  $f_1^u$  and  $f_1^d$ . In this approach  $f_1^d$  lies between the asymptotic and the BLW value;  $f_1^u$  is also close to the asymptotic or the BLW value, but its deviation from the asymptotic value is in the “wrong” direction. In Fig. 6 we show the electromagnetic form factors of the proton, in Fig. 7 the electromagnetic form factors of the neutron, in Fig. 8 the axial and the tensor form factor of the proton, and finally in Fig. 9 the ratio of the form factors  $F_2$  and  $F_1$  of the proton. In Fig. 10 we show the three  $N \rightarrow \Delta$  transition form factors. In all cases we obtain results which are very close to the BLW results of the previous section, so it seems that the nucleon form factors are very sensitive to the values of  $V_1^d$  and  $A_1^u$ , while the dependence on  $f_N/\lambda_1$ ,  $f_1^d$ , and  $f_1^u$  is less pronounced.

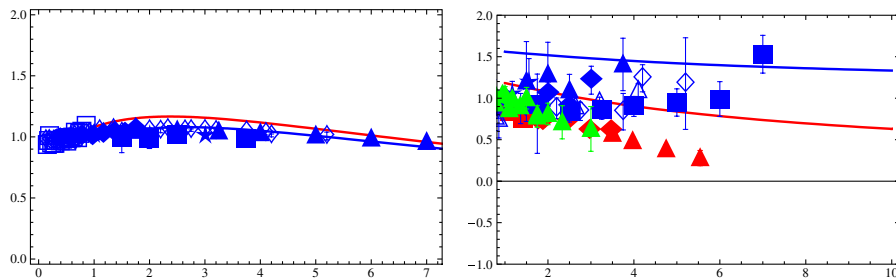


FIG. 6 (color online). LCSR results for the electromagnetic form factors [left panel:  $G_M/(\mu_p G_D)$  vs  $Q^2$ ; right panel:  $\mu_p G_E/G_M$  vs  $Q^2$ ] of the proton. In the left panel the upper (red) curve corresponds to the BLW model, and the lower (blue) curve is based on the lattice data. In the right panel the lower (red) curve corresponds to the BLW model, and the upper (blue) curve is based on the lattice data. In both models the parameters  $f_1^x$  are determined from the twist-3 parameters, cf. Eq. (47). The red (gray) triangles in the right panel are JLAB data, while the dark gray (blue) data points and the light gray (green) triangles are obtained via Rosenbluth separation.

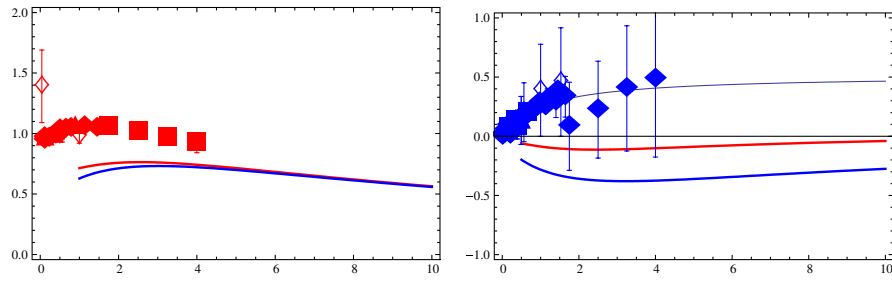


FIG. 7 (color online). LCSR results for the electromagnetic form factors of the neutron [left panel:  $G_M/(\mu_n G_D)$  vs  $Q^2$ ; right panel:  $G_E/(G_D)$  vs  $Q^2$ ]. The upper (red) curves correspond to the BLW model, and the lower (blue) curves are based on the lattice data. In both models the parameters  $f_1^x$  are determined from the twist-3 parameters, cf. Eq. (47). The thin solid (blue) line represents the updated Galster fit.

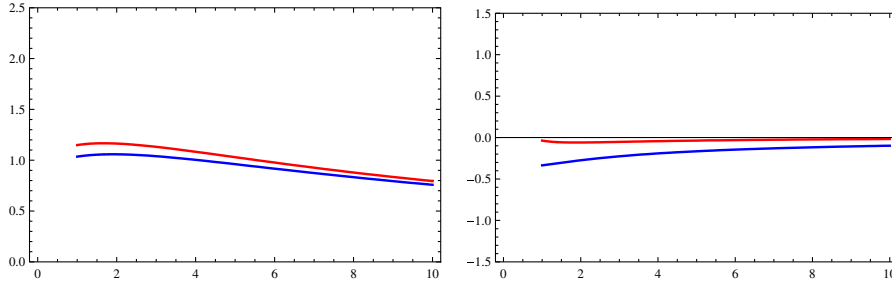


FIG. 8 (color online). LCSR results for the axial form factor of the proton  $G_A$  normalized to  $G_D = g_A/(1 + Q^2/m_A^2)^2$  vs  $Q^2$  (left panel) and the tensor form factor  $G_T$  normalized to  $G_A$  vs  $Q^2$  (right panel). The upper (red) curves correspond to the BLW model, and the lower (blue) curves are based on the lattice data. In both models the parameters  $f_1^x$  are determined from the twist-3 parameters, cf. Eq. (47).

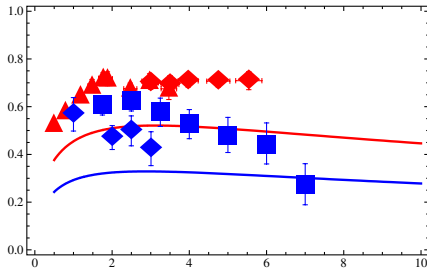


FIG. 9 (color online). LCSR results for the ratio  $\sqrt{Q^2} F_2^p / (F_1^p * 1.79)$ . The upper (red) curve corresponds to the BLW model, and the lower (blue) curve is based on the lattice data. In both models the parameters  $f_1^x$  are determined from the twist-3 parameters, cf. Eq. (47). Gray (red) symbols: experimental values obtained via polarization transfer. Dark gray (blue) symbols: experimental values obtained via Rosenbluth separation.

## IX. EFFECTS OF HIGHER CONFORMAL SPIN CONTRIBUTIONS

In this section we include (in comparison to the previous sections) also contributions of the next-to-next-to-leading conformal spin to the leading-twist distribution amplitude. These terms have been determined on the lattice [3,4] and with QCD sum rules [29,30,37]. The explicit expressions for the leading-twist distribution amplitudes can be found in Appendix C. The contributions of these higher moments to the electromagnetic form factors of the nucleon have already been estimated in [16], but only for the Chernyak-Zhitnitsky interpolating field. Here we work out the contributions of the second moments to the light-cone sum rules for nucleon form factors using the Ioffe current. We

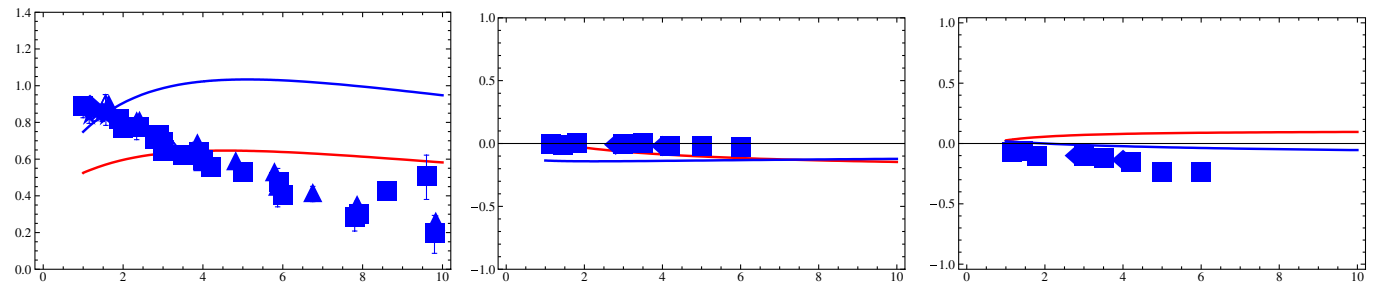


FIG. 10 (color online).  $\gamma^* N \rightarrow \Delta$  transition form factors [left panel:  $G_M^*/(3G_D)$  vs  $Q^2$ ; middle panel:  $R_{EM}$  vs  $Q^2$ ; right panel:  $R_{SM}$  vs  $Q^2$ ] in the LCSR approach [54]. In the left panel the upper (blue) curve is based on the lattice data, and the lower (red) curve corresponds to the BLW model. In the other panels the upper (red) curve corresponds to the BLW model, while the lower (blue) curve is based on the lattice data. In both models the parameters  $f_1^x$  are determined from the twist-3 parameters, cf. Eq. (47).

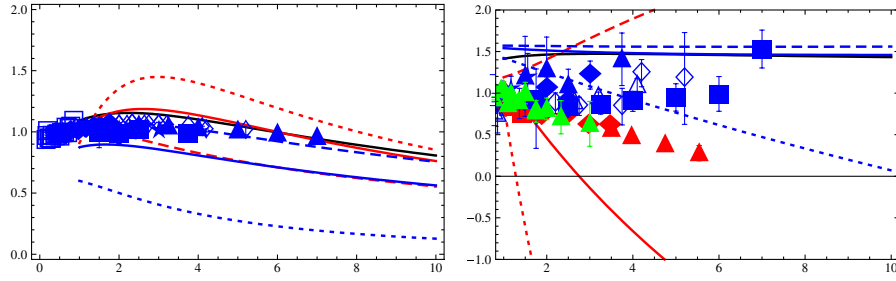


FIG. 11 (color online). LCSR results for the electromagnetic form factors [left panel:  $G_M/(\mu_p G_D)$  vs  $Q^2$ ; right panel:  $\mu_p G_E/G_M$  vs  $Q^2$ ] of the proton. In the left panel the curves correspond to the models (2), (1), (4), (6), (7), (3), and (5) (from top to bottom on the right). In the right panel the curves correspond to the models (3), (6), (7), (1), (5), (4), and (2) (from top to bottom on the right), where (7) and (1) are almost identical. The gray (red) triangles in the right panel are JLAB data, while the dark gray (blue) data points and the light gray (green) triangles are obtained via Rosenbluth separation.

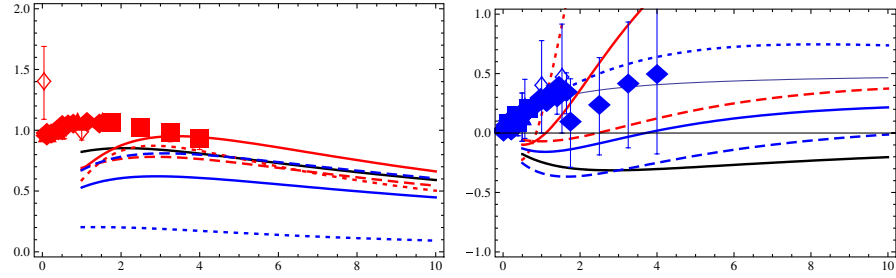


FIG. 12 (color online). LCSR results for the electromagnetic form factors of the neutron [left panel:  $G_M/(\mu_n G_D)$  vs  $Q^2$ ; right panel:  $G_E$  vs  $Q^2$ ]. In the left panel the curves correspond to the models (4), (6), (1), (3), (2), (7), and (5) (from top to bottom on the right). In the right panel the thick curves correspond to the models (2), (4), (5), (3), (7), (6), and (1) (from top to bottom on the right), while the thin solid (blue) line represents the updated Galster fit.

will use the form in Eq. (C1) for the leading-twist distribution amplitude and the following parameter sets:

- (1) asymptotic distribution amplitude (black lines in Figs. 11–15),
- (2) BLW plus second moments from QCD sum rules (dotted red lines),
- (3) BLW plus second moments from the lattice (dashed red lines),
- (4) BLW plus second moments *à la* BLW (solid red lines),

- (5) lattice evaluation plus QCD sum-rule estimates for  $f_x^y$  (dotted blue lines),
- (6) lattice evaluation plus asymptotic values for  $f_x^y$  (dashed blue lines),
- (7) lattice evaluation plus BLW estimates for  $f_x^y$  (solid blue lines).

In Fig. 11 we show the electromagnetic form factors of the proton, in Fig. 12 the electromagnetic form factors of the neutron, in Fig. 13 the axial and the tensor form factors of the proton, and finally in Fig. 14 the ratio of the form

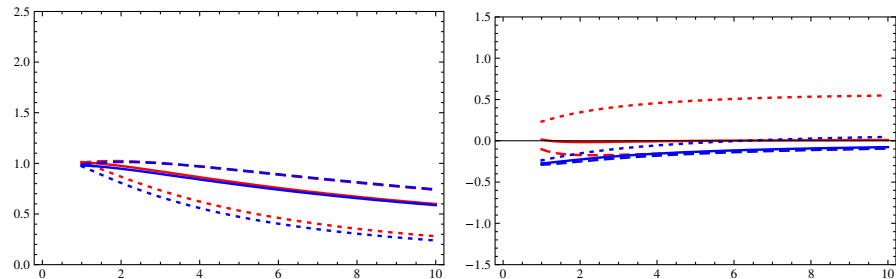


FIG. 13 (color online). LCSR results for the axial form factor of the proton  $G_A$  normalized to  $G_D = g_A/(1 + Q^2/m_A^2)$  vs  $Q^2$  (left panel) and the tensor form factor  $G_T$  normalized to  $G_A$  vs  $Q^2$  (right panel). In the left panel the curves correspond to the models (6), (3), (4), (7), (2), and (5) (from top to bottom on the right), where (6) and (3) as well as (4) and (7) are almost identical. In the right panel the curves correspond to the models (2), (5), (4), (7), (6), and (3) (from top to bottom on the right), where (4) yields nearly zero and (7), (6), and (3) are almost identical.

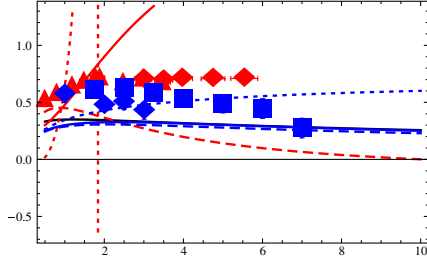


FIG. 14 (color online). LCSR results for the ratio  $\sqrt{Q^2} F_2^p / (F_1^p * 1.79)$ . The curves correspond to the models (4), (5), (1), (7), (6), (3), and (2) (from top to bottom on the right), where (1), (7), and (6) are almost identical. Gray (red) symbols: experimental values obtained via polarization transfer. Dark gray (blue) symbols: experimental values obtained via Rosenbluth separation.

factors  $F_2$  and  $F_1$  of the proton. In Fig. 15 we show the three  $N \rightarrow \Delta$  transition form factors.

In almost all cases the second moments of the leading-twist distribution amplitude determined with QCD sum rules give huge corrections. We show these parameter sets in the plots, but we will not discuss them any further.

The magnetic form factor of the proton  $G_M^p$  is very well described by the BLW model with second moments *à la* BLW [set (4)] or from the lattice [set (3)] and the lattice values for the distribution amplitude with  $f_x^y$  from BLW [set (7)] or with the asymptotic values for  $f_x^y$  [set (6)]. This is not unexpected, since the second moments *à la* BLW and from the lattice are quite similar in size. This observation ensures, however, that there is not an unexpected strong sensitivity of the LCSRs to the second moments. The theory predictions for the magnetic form factor of the neutron  $G_M^n$  are again shifted to lower values. Apart from this fact, the predictions for the parameter sets (1), (3), (4), (6), and (7) lie relatively close together and they agree a little better with experiment, compared to the case where the  $d$ -wave contributions have been neglected. Also for  $G_A^p$  and  $G_T^p$  we get nice results, unless we use the QCD sum-rule values of the second moments. As expected, in

$G_E^p/G_M^p$ ,  $G_E^n/G_D$ , and  $F_2^p/F_1^p$  cancellations arise that lead to a strong dependence on the concrete form of the nucleon distribution amplitudes.

In the case of the  $N \rightarrow \Delta$  transition the inclusion of  $d$ -wave corrections leads to strong enhancements in the prediction of  $G_M^*$ , while  $R_{EM}$  and  $R_{SM}$  agree now better with experiment.

## X. CONCLUSION

We have compared a new determination of the nucleon distribution amplitudes based on lattice QCD with different values available in the literature. The nonperturbative parameters of nonleading conformal spin from the lattice evaluation turned out to be close to the asymptotic form and very close to the BLW model. For the leading conformal spin parameters  $f_N$ ,  $\lambda_1$ , and  $\lambda_2$  the deviation between lattice and QCD sum rules is about 30%, which is possibly due to neglected radiative corrections in the QCD sum-rule estimates. Our models for the nucleon distribution amplitudes can be related to measurable form factors with light-cone sum rules. Despite the fact that the light-cone sum rules are only calculated to leading order in QCD and despite an intrinsic uncertainty of light-cone sum rules of about  $\pm 20\%$  we get a very good description of  $G_M^p$ ,  $G_M^n$ ,  $G_A^p$ , and  $G_T^p$  at intermediate momentum transfer. In  $G_E^p$ ,  $G_E^n$ , and  $F_2^p/F_1^p$  cancellations occur, which limit our predictive power. In general we found the following tendency: The asymptotic distribution amplitudes describe the data already amazingly well. Pure QCD sum-rule estimates for the nonperturbative parameters overestimate the deviation from the asymptotic form, but the deviation goes in the right direction. The best results are obtained for the BLW values and the very similar lattice values. Including also  $d$ -wave contributions to the twist-3 distribution amplitude improves the description of  $G_M^p$ ,  $G_M^n$ ,  $G_A^p$ , and  $G_T^p$  a little bit, but results also in bigger uncertainties in  $G_E^p$ ,  $G_E^n$ , and  $F_2^p/F_1^p$ . In the case of the  $N \rightarrow \Delta$  transition, we do not see the steep falloff of  $G_M^*$ , but the smallness of  $R_{EM}$  and  $R_{SM}$  is very well reproduced.

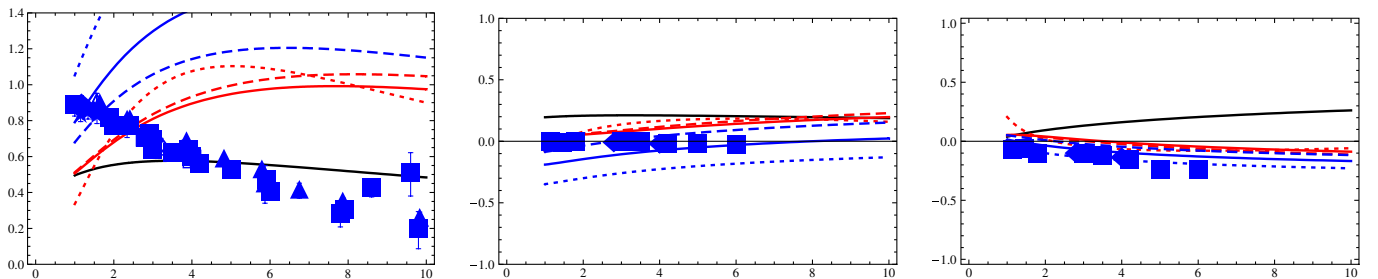


FIG. 15 (color online).  $\gamma^* N \rightarrow \Delta$  transition form factors [left panel:  $G_M^*/(3G_D)$  vs  $Q^2$ ; middle panel:  $R_{EM}$  vs  $Q^2$ ; right panel:  $R_{SM}$  vs  $Q^2$ ] in the LCSR approach [54]. In the left panel the curves correspond to the models (5), (7), (6), (3), (4), (2), and (1) (from top to bottom on the right). In the middle panel the curves correspond to the models (1), (2), (3), (4), (6), (7), and (5) (from top to bottom on the left), where (3) and (4) are almost identical. In the right panel the curves correspond to the models (1), (2), (4), (3), (6), (7), and (5) (from top to bottom on the right), where (3) and (6) are almost identical.

Further improvements on the theoretical side can be achieved by determining the NLO-QCD corrections to light-cone sum rules, which connect the nucleon distribution amplitudes to the form factors. To match the NLO-QCD accuracy also  $\alpha_s$  corrections have then to be included in all QCD sum-rule estimates of the moments of the nucleon distribution amplitudes.

### ACKNOWLEDGMENTS

We would like to thank V. Braun and A. Schäfer for discussions and comments on the manuscript, R. Schiavilla for providing the data for  $G_E^n$  from Ref. [101], and Y. Aoki for clarifying comments. All lattice data were provided by

the QCDSF Collaboration. This work was supported by DFG (Forschergruppe Gitter-Hadronen-Phänomenologie and SFB/TR55 Hadron Physics from Lattice QCD) and by BMBF.

### APPENDIX A: NUCLEON DISTRIBUTION AMPLITUDES UP TO TWIST 6

For completeness we give in this Appendix the full expressions for the nucleon distribution amplitudes up to twist 6; details can be found in [2,6]. The general Lorentz decomposition of the matrix element defined in Eq. (5) reads [2]

$$\begin{aligned}
4\langle 0 | \epsilon^{ijk} u_\alpha^i(a_1 x) u_\beta^j(a_2 x) d_\gamma^k(a_3 x) | P \rangle = & S_1 m_N C_{\alpha\beta}(\gamma_5 N)_\gamma + S_2 m_N^2 C_{\alpha\beta}(\not{x} \gamma_5 N)_\gamma + \mathcal{P}_1 m_N (\gamma_5 C)_{\alpha\beta} N_\gamma + \mathcal{P}_2 m_N^2 (\gamma_5 C)_{\alpha\beta} (\not{x} N)_\gamma \\
& + \left( \mathcal{V}_1 + \frac{x^2 m_N^2}{4} \mathcal{V}_1^M \right) (\not{P} C)_{\alpha\beta} (\gamma_5 N)_\gamma + \mathcal{V}_2 m_N (\not{P} C)_{\alpha\beta} (\not{x} \gamma_5 N)_\gamma + \mathcal{V}_3 m_N (\gamma_\mu C)_{\alpha\beta} \\
& \times (\gamma^\mu \gamma_5 N)_\gamma + \mathcal{V}_4 m_N^2 (\not{x} C)_{\alpha\beta} (\gamma_5 N)_\gamma + \mathcal{V}_5 m_N^2 (\gamma_\mu C)_{\alpha\beta} (i\sigma^{\mu\nu} x_\nu \gamma_5 N)_\gamma \\
& + \mathcal{V}_6 m_N^3 (\not{x} C)_{\alpha\beta} (\not{x} \gamma_5 N)_\gamma + \left( \mathcal{A}_1 + \frac{x^2 m_N^2}{4} \mathcal{A}_1^M \right) (\not{P} \gamma_5 C)_{\alpha\beta} N_\gamma \\
& + \mathcal{A}_2 m_N (\not{P} \gamma_5 C)_{\alpha\beta} (\not{x} N)_\gamma + \mathcal{A}_3 m_N (\gamma_\mu \gamma_5 C)_{\alpha\beta} (\gamma^\mu N)_\gamma + \mathcal{A}_4 m_N^2 (\not{x} \gamma_5 C)_{\alpha\beta} N_\gamma \\
& + \mathcal{A}_5 m_N^2 (\gamma_\mu \gamma_5 C)_{\alpha\beta} (i\sigma^{\mu\nu} x_\nu N)_\gamma + \mathcal{A}_6 m_N^3 (\not{x} \gamma_5 C)_{\alpha\beta} (\not{x} N)_\gamma + \left( \mathcal{T}_1 + \frac{x^2 m_N^2}{4} \mathcal{T}_1^M \right) \\
& \times (P^\nu i\sigma_{\mu\nu} C)_{\alpha\beta} (\gamma^\mu \gamma_5 N)_\gamma + \mathcal{T}_2 m_N (x^\mu P^\nu i\sigma_{\mu\nu} C)_{\alpha\beta} (\gamma_5 N)_\gamma \\
& + \mathcal{T}_3 m_N (\sigma_{\mu\nu} C)_{\alpha\beta} (\sigma^{\mu\nu} \gamma_5 N)_\gamma + \mathcal{T}_4 m_N (P^\nu \sigma_{\mu\nu} C)_{\alpha\beta} (\sigma^{\mu\rho} x_\rho \gamma_5 N)_\gamma \\
& + \mathcal{T}_5 m_N^2 (x^\nu i\sigma_{\mu\nu} C)_{\alpha\beta} (\gamma^\mu \gamma_5 N)_\gamma + \mathcal{T}_6 m_N^2 (x^\mu P^\nu i\sigma_{\mu\nu} C)_{\alpha\beta} (\not{x} \gamma_5 N)_\gamma \\
& + \mathcal{T}_7 m_N^2 (\sigma_{\mu\nu} C)_{\alpha\beta} (\sigma^{\mu\nu} \not{x} \gamma_5 N)_\gamma + \mathcal{T}_8 m_N^3 (x^\nu \sigma_{\mu\nu} C)_{\alpha\beta} (\sigma^{\mu\rho} x_\rho \gamma_5 N)_\gamma, \tag{A1}
\end{aligned}$$

with

$$\begin{aligned}
S_1 = S_1, \quad 2(P \cdot x)S_2 = S_1 - S_2, \quad \mathcal{P}_1 = P_1, \quad 2(P \cdot x)\mathcal{P}_2 = P_2 - P_1, \\
\mathcal{V}_1 = V_1, \quad 2(P \cdot x)\mathcal{V}_2 = V_1 - V_2 - V_3, \quad 2\mathcal{V}_3 = V_3, \quad 4(P \cdot x)\mathcal{V}_4 = -2V_1 + V_3 + V_4 + 2V_5, \\
4(P \cdot x)\mathcal{V}_5 = V_4 - V_3, \quad 4(P \cdot x)^2\mathcal{V}_6 = -V_1 + V_2 + V_3 + V_4 + V_5 - V_6, \\
\mathcal{A}_1 = A_1, \quad 2(P \cdot x)\mathcal{A}_2 = -A_1 + A_2 - A_3, \quad 2\mathcal{A}_3 = A_3, \quad 4(P \cdot x)\mathcal{A}_4 = -2A_1 - A_3 - A_4 + 2A_5, \\
4(P \cdot x)\mathcal{A}_5 = A_3 - A_4, \quad 4(P \cdot x)^2\mathcal{A}_6 = A_1 - A_2 + A_3 + A_4 - A_5 + A_6, \\
\mathcal{T}_1 = T_1, \quad 2(P \cdot x)\mathcal{T}_2 = T_1 + T_2 - 2T_3, \quad 2\mathcal{T}_3 = T_7, \quad 2(P \cdot x)\mathcal{T}_4 = T_1 - T_2 - 2T_7, \\
2(P \cdot x)\mathcal{T}_5 = -T_1 + T_5 + 2T_8, \quad 4(P \cdot x)^2\mathcal{T}_6 = 2T_2 - 2T_3 - 2T_4 + 2T_5 + 2T_7 + 2T_8, \\
4(P \cdot x)\mathcal{T}_7 = T_7 - T_8, \quad 4(P \cdot x)^2\mathcal{T}_8 = -T_1 + T_2 + T_5 - T_6 + 2T_7 + 2T_8. \tag{A2}
\end{aligned}$$

The calligraphic notation is used for distribution amplitudes belonging to a simple Dirac structure, while the noncalligraphic functions denote distribution amplitudes of definite twist. Each distribution amplitude  $F = V_i, A_i, T_i, S_i$ , and  $P_i$  can be represented as

$$F(a_1, a_2, a_3, (P \cdot x)) = \int \mathcal{D}x e^{-i(P \cdot x) \sum_i x_i a_i} F(x_i), \tag{A3}$$

where the functions  $F(x_i)$  depend on the dimensionless variables  $x_i$ ,  $0 < x_i < 1$ , and  $\sum_i x_i = 1$  which correspond to the longitudinal momentum fractions carried by the quarks inside the nucleon.

**APPENDIX B: EXPANSION OF THE NUCLEON DISTRIBUTION AMPLITUDES UP TO NEXT-TO-LEADING CONFORMAL SPIN**

In [2] the distribution amplitudes were expanded up to next-to-leading order in the conformal spin. The twist-3 distribution amplitudes read

$$\begin{aligned} V_1(x_i, \mu) &= 120x_1x_2x_3[\phi_3^0(\mu) + \phi_3^+(\mu)(1 - 3x_3)], & A_1(x_i, \mu) &= 120x_1x_2x_3(x_2 - x_1)\phi_3^-(\mu), \\ T_1(x_i, \mu) &= 120x_1x_2x_3[\phi_3^0(\mu) - \frac{1}{2}(\phi_3^+ - \phi_3^-)(\mu)(1 - 3x_3)]. \end{aligned} \quad (\text{B1})$$

The twist-4 distribution amplitudes read

$$\begin{aligned} V_2(x_i, \mu) &= 24x_1x_2[\phi_4^0(\mu) + \phi_4^+(\mu)(1 - 5x_3)], \\ A_2(x_i, \mu) &= 24x_1x_2(x_2 - x_1)\phi_4^-(\mu), \\ T_2(x_i, \mu) &= 24x_1x_2[\xi_4^0(\mu) + \xi_4^+(\mu)(1 - 5x_3)], \\ V_3(x_i, \mu) &= 12x_3[\psi_4^0(\mu)(1 - x_3) + \psi_4^+(\mu)(1 - x_3 - 10x_1x_2) + \psi_4^-(\mu)(x_1^2 + x_2^2 - x_3(1 - x_3))], \\ A_3(x_i, \mu) &= 12x_3(x_2 - x_1)[(\psi_4^0 + \psi_4^+)(\mu) + \psi_4^-(\mu)(1 - 2x_3)], \\ T_3(x_i, \mu) &= 6x_3[(\phi_4^0 + \psi_4^0 + \xi_4^0)(\mu)(1 - x_3) + (\phi_4^+ + \psi_4^+ + \xi_4^+)(\mu)(1 - x_3 - 10x_1x_2) \\ &\quad + (\phi_4^- - \psi_4^- + \xi_4^-)(\mu)(x_1^2 + x_2^2 - x_3(1 - x_3))], \\ T_7(x_i, \mu) &= 6x_3[(\phi_4^0 + \psi_4^0 - \xi_4^0)(\mu)(1 - x_3) + (\phi_4^+ + \psi_4^+ - \xi_4^+)(\mu)(1 - x_3 - 10x_1x_2) \\ &\quad + (\phi_4^- - \psi_4^- - \xi_4^-)(\mu)(x_1^2 + x_2^2 - x_3(1 - x_3))], \\ S_1(x_i, \mu) &= 6x_3(x_2 - x_1)[(\phi_4^0 + \psi_4^0 + \xi_4^0 + \phi_4^+ + \psi_4^+ + \xi_4^+)(\mu) + (\phi_4^- - \psi_4^- + \xi_4^-)(\mu)(1 - 2x_3)], \\ P_1(x_i, \mu) &= 6x_3(x_1 - x_2)[(\phi_4^0 + \psi_4^0 - \xi_4^0 + \phi_4^+ + \psi_4^+ - \xi_4^+)(\mu) + (\phi_4^- - \psi_4^- - \xi_4^-)(\mu)(1 - 2x_3)]. \end{aligned} \quad (\text{B2})$$

The twist-5 amplitudes are given by

$$\begin{aligned} V_4(x_i, \mu) &= 3[\psi_5^0(\mu)(1 - x_3) + \psi_5^+(\mu)(1 - x_3 - 2(x_1^2 + x_2^2)) + \psi_5^-(\mu)(2x_1x_2 - x_3(1 - x_3))], \\ A_4(x_i, \mu) &= 3(x_2 - x_1)[-\psi_5^0(\mu) + \psi_5^+(\mu)(1 - 2x_3) + \psi_5^-(\mu)x_3], \\ T_4(x_i, \mu) &= \frac{3}{2}[(\phi_5^0 + \psi_5^0 + \xi_5^0)(\mu)(1 - x_3) + (\phi_5^+ + \psi_5^+ + \xi_5^+)(\mu)(1 - x_3 - 2(x_1^2 + x_2^2)) \\ &\quad + (\phi_5^- - \psi_5^- + \xi_5^-)(\mu)(2x_1x_2 - x_3(1 - x_3))], \\ T_8(x_i, \mu) &= \frac{3}{2}[(\phi_5^0 + \psi_5^0 - \xi_5^0)(\mu)(1 - x_3) + (\phi_5^+ + \psi_5^+ - \xi_5^+)(\mu)(1 - x_3 - 2(x_1^2 + x_2^2)) \\ &\quad + (\phi_5^- - \psi_5^- - \xi_5^-)(\mu)(2x_1x_2 - x_3(1 - x_3))], \\ V_5(x_i, \mu) &= 6x_3[\phi_5^0(\mu) + \phi_5^+(\mu)(1 - 2x_3)], \\ A_5(x_i, \mu) &= 6x_3(x_2 - x_1)\phi_5^-(\mu), \\ T_5(x_i, \mu) &= 6x_3[\xi_5^0(\mu) + \xi_5^+(\mu)(1 - 2x_3)], \\ S_2(x_i, \mu) &= \frac{3}{2}(x_2 - x_1)[-(\phi_5^0 + \psi_5^0 + \xi_5^0)(\mu) + (\phi_5^+ + \psi_5^+ + \xi_5^+)(\mu)(1 - 2x_3) + (\phi_5^- - \psi_5^- + \xi_5^-)(\mu)x_3], \\ P_2(x_i, \mu) &= \frac{3}{2}(x_2 - x_1)[-(\phi_5^0 - \psi_5^0 + \xi_5^0)(\mu) + (-\phi_5^+ - \psi_5^+ + \xi_5^+)(\mu)(1 - 2x_3) + (-\phi_5^- + \psi_5^- + \xi_5^-)(\mu)x_3], \end{aligned} \quad (\text{B3})$$

and the twist-6 contributions are given by

$$\begin{aligned} V_6(x_i, \mu) &= 2[\phi_6^0(\mu) + \phi_6^+(\mu)(1 - 3x_3)], \\ A_6(x_i, \mu) &= 2(x_2 - x_1)\phi_6^-, \\ T_6(x_i, \mu) &= 2[\phi_6^0(\mu) - \frac{1}{2}(\phi_6^+ - \phi_6^-)(1 - 3x_3)]. \end{aligned} \quad (\text{B4})$$

The coefficients  $\phi_i^x$ ,  $\psi_i^x$ , and  $\xi_i^x$  ( $i$  stands for the twist) in the above expansions can be expressed in terms of the eight nonperturbative parameters  $f_N$ ,  $\lambda_1$ ,  $\lambda_2$ ,  $f_1^u$ ,  $f_1^d$ ,  $f_2^d$ ,  $A_1^u$ , and

$V_1^d$ , defined in Sec. II. The corresponding relations read, for the leading conformal spin,

$$\begin{aligned} \phi_3^0 &= \phi_6^0 = f_N, & \phi_4^0 &= \phi_5^0 = \frac{1}{2}(f_N + \lambda_1), \\ \xi_4^0 &= \xi_5^0 = \frac{1}{6}\lambda_2, & \psi_4^0 &= \psi_5^0 = \frac{1}{2}(f_N - \lambda_1). \end{aligned} \quad (\text{B5})$$

For the next-to-leading spin, for twist 3:

$$\phi_3^- = \frac{2}{2}f_N A_1^u, \quad \phi_3^+ = \frac{7}{2}f_N(1 - 3V_1^d), \quad (\text{B6})$$

for twist 4:

$$\begin{aligned}
\phi_4^+ &= \frac{1}{4}[f_N(3 - 10V_1^d) + \lambda_1(3 - 10f_1^d)], \\
\phi_4^- &= -\frac{5}{4}[f_N(1 - 2A_1^u) - \lambda_1(1 - 2f_1^d - 4f_1^u)], \\
\psi_4^+ &= -\frac{1}{4}[f_N(2 + 5A_1^u - 5V_1^d) - \lambda_1(2 - 5f_1^d - 5f_1^u)], \\
\psi_4^- &= \frac{5}{4}[f_N(2 - A_1^u - 3V_1^d) - \lambda_1(2 - 7f_1^d + f_1^u)], \\
\xi_4^+ &= \frac{1}{16}\lambda_2(4 - 15f_2^d), \quad \xi_4^- = \frac{5}{16}\lambda_2(4 - 15f_2^d), \quad (\text{B7})
\end{aligned}$$

for twist 5:

$$\begin{aligned}
\phi_5^+ &= -\frac{5}{6}[f_N(3 + 4V_1^d) - \lambda_1(1 - 4f_1^d)], \\
\phi_5^- &= -\frac{5}{3}[f_N(1 - 2A_1^u) - \lambda_1(f_1^d - f_1^u)], \\
\psi_5^+ &= -\frac{5}{6}[f_N(5 + 2A_1^u - 2V_1^d) - \lambda_1(1 - 2f_1^d - 2f_1^u)], \\
\psi_5^- &= \frac{5}{3}[f_N(2 - A_1^u - 3V_1^d) + \lambda_1(f_1^d - f_1^u)], \\
\xi_5^+ &= \frac{5}{36}\lambda_2(2 - 9f_2^d), \quad \xi_5^- = -\frac{5}{4}\lambda_2f_2^d, \quad (\text{B8})
\end{aligned}$$

and for twist 6:

$$\begin{aligned}
C_f^u &= (1 - x_2)^3[113 + 495x_2 - 552x_2^2 - 10A_1^u(1 - 3x_2) + 2V_1^d(113 - 951x_2 + 828x_2^2)], \\
C_\lambda^u &= -(1 - x_2)^3[13 - 20f_1^d + 3x_2 + 10f_1^u(1 - 3x_2)], \\
C_f^d &= -(1 - x_3)[1441 + 505x_3 - 3371x_3^2 + 3405x_3^3 - 1104x_3^4 - 24V_1^d(207 - 3x_3 - 368x_3^2 + 412x_3^3 - 138x_3^4)] \\
&\quad - 12(73 - 220V_1^d)\ln(x_3), \\
C_\lambda^d &= -(1 - x_3)[11 + 131x_3 - 169x_3^2 + 63x_3^3 - 30f_1^d(3 + 11x_3 - 17x_3^2 + 7x_3^3)] - 12(3 - 10f_1^d)\ln(x_3). \quad (\text{B11})
\end{aligned}$$

In the case of  $A_1$  one finds

$$\begin{aligned}
\mathcal{A}_1^{M(u)}(x_2) &= \int_0^{1-x_2} dx_1 A_1^M(x_1, x_2, 1 - x_1 - x_2) = \frac{x_2^2}{24}(1 - x_2)^3(f_N D_f^u + \lambda_1 D_\lambda^u), \\
\mathcal{A}_1^{M(d)}(x_3) &= \int_0^{1-x_3} dx_1 A_1^M(x_1, 1 - x_1 - x_3, x_3) = 0,
\end{aligned} \quad (\text{B12})$$

with

$$\begin{aligned}
D_f^u &= 11 + 45x_2 - 2A_1^u(113 - 951x_2 + 828x_2^2) + 10V_1^d(1 - 30x_2), \\
D_\lambda^u &= 29 - 45x_2 - 10f_1^u(7 - 9x_2) - 20f_1^d(5 - 6x_2).
\end{aligned} \quad (\text{B13})$$

Finally, for  $T_1$  one has

$$\begin{aligned}
\mathcal{T}_1^{M(u)}(x_2) &= \int_0^{1-x_2} dx_1 T_1^M(x_1, x_2, 1 - x_1 - x_2) = \frac{x_2^2}{48}(f_N E_f^u + \lambda_1 E_\lambda^u), \\
\mathcal{T}_1^{M(d)}(x_3) &= \int_0^{1-x_3} dx_1 T_1^M(x_1, 1 - x_1 - x_3, x_3) = \frac{x_3^2(1 - x_3)^4}{4}(f_N E_f^d + \lambda_1 E_\lambda^d)
\end{aligned} \quad (\text{B14})$$

with

$$\begin{aligned}
E_f^u &= -[(1 - x_2)(3(439 + 71x_2 - 621x_2^2 + 587x_2^3 - 184x_2^4) + 4A_1^u(1 - x_2)^2(59 - 483x_2 + 414x_2^2) \\
&\quad - 4V_1^d(1301 - 619x_2 - 769x_2^2 + 1161x_2^3 - 414x_2^4))] - 12(73 - 220V_1^d)\ln(x_2), \\
E_\lambda^u &= -[(1 - x_2)(5 - 211x_2 + 281x_2^2 - 111x_2^3 + 10(1 + 61x_2 - 83x_2^2 + 33x_2^3)f_1^d - 40(1 - x_2)^2(2 - 3x_2)f_1^u)] \\
&\quad - 12(3 - 10f_1^d)\ln(x_2), \\
E_f^d &= 17 + 92x_3 + 12(A_1^u + V_1^d)(3 - 23x_3), \\
E_\lambda^d &= -7 + 20f_1^d + 10f_1^u. \quad (\text{B15})
\end{aligned}$$

$$\begin{aligned}
\phi_6^+ &= \frac{1}{2}[f_N(1 - 4V_1^d) - \lambda_1(1 - 2f_1^d)], \\
\phi_6^- &= \frac{1}{2}[f_N(1 + 4A_1^u) + \lambda_1(1 - 4f_1^d - 2f_1^u)].
\end{aligned} \quad (\text{B9})$$

Next we summarize the expressions for the  $x^2$  corrections to the leading-twist distribution amplitudes  $V_1$ ,  $A_1$ , and  $T_1$ . These corrections have been determined in [6,16,27,28]. For  $V_1$  we have

$$\begin{aligned}
\mathcal{V}_1^{M(u)}(x_2) &= \int_0^{1-x_2} dx_1 V_1^M(x_1, x_2, 1 - x_1 - x_2) \\
&= \frac{x_2^2}{24}(f_N C_f^u + \lambda_1 C_\lambda^u), \\
\mathcal{V}_1^{M(d)}(x_3) &= \int_0^{1-x_3} dx_1 V_1^M(x_1, 1 - x_1 - x_3, x_3) \\
&= \frac{x_3^2}{24}(f_N C_f^d + \lambda_1 C_\lambda^d)
\end{aligned} \quad (\text{B10})$$

with

**APPENDIX C: EXPANSION OF THE NUCLEON DISTRIBUTION AMPLITUDE OF TWIST 3 UP TO NEXT-TO-NEXT-TO-LEADING CONFORMAL SPIN**

The expansion of the leading-twist distribution amplitude in a basis which is diagonal with respect to one-loop renormalization reads up to next-to-next-to-leading conformal spin

$$\begin{aligned} \varphi(x_1, x_2, x_3, \mu) = & 120x_1x_2x_3f_N(\mu_0)L^{2/3\beta_0}\{1 + h_{10}(\mu_0)(x_1 - 2x_2 + x_3)L^{8/3\beta_0} + h_{11}(\mu_0)(x_1 - x_3)L^{20/9\beta_0} \\ & + h_{20}(\mu_0)[1 + 7(x_2 - 2x_1x_3 - 2x_2^2)]L^{14/3\beta_0} + h_{21}(\mu_0)(1 - 4x_2)(x_1 - x_3)L^{40/9\beta_0} \\ & + h_{22}(\mu_0)[3 - 9x_2 + 8x_2^2 - 12x_1x_3]L^{32/9\beta_0}\} \end{aligned} \quad (C1)$$

with

$$L = \frac{\alpha_s(\mu)}{\alpha_s(\mu_0)}, \quad \beta_0 = 11 - \frac{2}{3}n_F. \quad (C2)$$

The coefficients  $h_{ij}$  can be expressed in terms of the moments by

$$h_{10}(\mu) = \frac{7}{2}(1 - 3\varphi^{010}(\mu)) \quad (C3)$$

$$= -\frac{7}{4}(1 - 3(A_1^u(\mu) + V_1^d(\mu))) \quad (C4)$$

$$= -\frac{1}{2}(\tilde{\phi}_3^+(\mu) - \tilde{\phi}_3^-(\mu)), \quad (C5)$$

$$h_{11}(\mu) = \frac{21}{2}(\varphi^{100}(\mu) - \varphi^{001}(\mu)) \quad (C6)$$

$$= \frac{21}{4}(1 + A_1^u(\mu) - 3V_1^d(\mu)) \quad (C7)$$

$$= \frac{1}{2}(3\tilde{\phi}_3^+(\mu) + \tilde{\phi}_3^-(\mu)), \quad (C8)$$

$$\begin{aligned} h_{20}(\mu) = & \frac{18}{5}(h_{10}(\mu) + 4 - 7(3\varphi^{101}(\mu) + \varphi^{200}(\mu) \\ & + \varphi^{002}(\mu))), \end{aligned} \quad (C9)$$

$$h_{21}(\mu) = 126(\varphi^{200}(\mu) - \varphi^{002}(\mu)) - 9h_{11}(\mu), \quad (C10)$$

$$\begin{aligned} h_{22}(\mu) = & \frac{21}{5}(-h_{10}(\mu) - 4 + 6(\varphi^{101}(\mu) + 2\varphi^{200}(\mu) \\ & + 2\varphi^{002}(\mu))). \end{aligned} \quad (C11)$$

Of course, this form of  $\varphi$  is not uniquely determined by the moments. The anomalous dimensions were obtained, e.g.,

in [115–117]. One can also write down the renormalization group equations for the moments  $\varphi^{n_1n_2n_3} = V_1^{n_1n_2n_3} - A_1^{n_1n_2n_3}$  alone:

$$\varphi^{100}(\mu) = \frac{1}{21}(7 + h_{10}(\mu_0)L^{8/3\beta_0} + h_{11}(\mu_0)L^{20/9\beta_0}), \quad (C12)$$

$$\varphi^{010}(\mu) = \frac{1}{21}(7 - 2h_{10}(\mu_0)L^{8/3\beta_0}), \quad (C13)$$

$$\varphi^{001}(\mu) = \frac{1}{21}(7 + h_{10}(\mu_0)L^{8/3\beta_0} - h_{11}(\mu_0)L^{20/9\beta_0}), \quad (C14)$$

$$\begin{aligned} \varphi^{101}(\mu) = & \frac{1}{126}(12 + 3h_{10}(\mu_0)L^{8/3\beta_0} - 2h_{20}(\mu_0)L^{14/3\beta_0} \\ & - h_{22}(\mu_0)L^{32/9\beta_0}), \end{aligned} \quad (C15)$$

$$\begin{aligned} \varphi^{200}(\mu) = & \frac{1}{252}(36 + 9h_{10}(\mu_0)L^{8/3\beta_0} + 9h_{11}(\mu_0)L^{20/9\beta_0} \\ & + h_{20}(\mu_0)L^{14/3\beta_0} + h_{21}(\mu_0)L^{40/9\beta_0} \\ & + 3h_{22}(\mu_0)L^{32/9\beta_0}), \end{aligned} \quad (C16)$$

$$\begin{aligned} \varphi^{002}(\mu) = & \frac{1}{252}(36 + 9h_{10}(\mu_0)L^{8/3\beta_0} - 9h_{11}(\mu_0)L^{20/9\beta_0} \\ & + h_{20}(\mu_0)L^{14/3\beta_0} - h_{21}(\mu_0)L^{40/9\beta_0} \\ & + 3h_{22}(\mu_0)L^{32/9\beta_0}). \end{aligned} \quad (C17)$$

Next we determine  $V_1$ ,  $A_1$ , and  $T_1$  from  $\varphi$  up to  $d$ -wave contributions. Including all anomalous dimensions we obtain (in the following we suppress the explicit renormalization scale dependence in the formulas)

$$\begin{aligned} V_1(x_1, x_2, x_3) = & 120x_1x_2x_3f_NL^{2/3\beta_0}\left\{1 - \frac{h_{10}}{2}(1 - 3x_3)L^{8/3\beta_0} + \frac{h_{11}}{2}(1 - 3x_3)L^{20/9\beta_0} \right. \\ & - \frac{h_{20}}{2}[(-2 + 7(x_1 + x_2 - 4x_1x_2))]L^{14/3\beta_0} - \frac{h_{21}}{2}[-1 + 8x_2 - 8x_2^2 - x_3 - 8x_2x_3 + 4x_3^2]L^{40/9\beta_0} \\ & \left. + \frac{h_{22}}{2}[6 - 21x_1 + 20x_1^2 - 21x_2 + 24x_1x_2 + 20x_2^2]L^{32/9\beta_0}\right\}, \end{aligned} \quad (C18)$$

$$A_1(x_1, x_2, x_3) = -60x_1x_2x_3(x_1 - x_2)f_N L^{2/3\beta_0} \{3h_{10}L^{8/3\beta_0} + h_{11}L^{20/9\beta_0} + (1 - 4x_3)(7h_{20}L^{14/3\beta_0} + h_{21}L^{40/9\beta_0} + h_{22}L^{32/9\beta_0})\}, \quad (\text{C19})$$

$$T_1(x_1, x_2, x_3) = 120x_1x_2x_3f_N L^{2/3\beta_0} \times \{1 + h_{10}(1 - 3x_3)L^{8/3\beta_0} - h_{20}[-1 + 14x_1x_2 - 7x_3 + 14x_3^2]L^{14/3\beta_0} - h_{22}[-3 + 12x_1x_2 + 9x_3 - 8x_3^2]L^{32/9\beta_0}\}. \quad (\text{C20})$$

In the light-cone sum-rule determination of the nucleon form factors we need the distribution amplitudes at a certain renormalization scale  $\mu = \mu_0$ ; therefore we give also the simplified expressions ( $L \equiv 1$ ) in the following. Our expressions agree up to next-to-leading conformal spin with the corresponding ones of [2]. In [16] the vector function  $V_1$  including the next-to-next-to-leading conformal spin was used with the following notation:

$$V_1(x_1, x_2, x_3) = 120x_1x_2x_3f_N [1 + \tilde{\phi}_3^+(1 - 3x_3) + \tilde{\phi}_3^{d1}[3 - 21x_3 + 28x_3^2] + \tilde{\phi}_3^{d2}[5(x_1^2 + x_2^2) - 3(1 - x_3)^2]], \quad (\text{C21})$$

$$A_1(x_1, x_2, x_3) = 120x_1x_2x_3(x_2 - x_1)f_N \times \{\tilde{\phi}_3^- + (1 - 4x_3)\tilde{\phi}_3^{d3}\}, \quad (\text{C22})$$

$$T_1(x_1, x_2, x_3) = 120x_1x_2x_3f_N \{1 + \frac{1}{2}(\tilde{\phi}_3^- - \tilde{\phi}_3^+)(1 - 3x_3) + \tilde{\phi}_3^{d4}[1 - 14x_1x_2 + 7x_3 - 14x_3^2] + \tilde{\phi}_3^{d5}[1 + x_1x_2 - 8x_3 + 11x_3^2]\}, \quad (\text{C23})$$

with

$$\tilde{\phi}_3^{d1} = \frac{1}{10}(h_{20} - h_{21} + 3h_{22}) \quad (\text{C24})$$

$$= \frac{9}{10}(3 + 28\varphi^{002} - 21V_1^d), \quad (\text{C25})$$

$$\tilde{\phi}_3^{d2} = \frac{1}{5}(-7h_{20} + 2h_{21} + 4h_{22}) \quad (\text{C26})$$

$$= -\frac{63}{5}(3 + 5A_1^u - V_1^d - 2(\varphi^{002} + 5\varphi^{101} + 5\varphi^{200})), \quad (\text{C27})$$

$$\tilde{\phi}_3^{d3} = \frac{1}{2}(7h_{20} + h_{21} + h_{22}) \quad (\text{C28})$$

$$= \frac{63}{2}(A_1^u + 4V_1^d - 4(\varphi^{002} + 2\varphi^{101})), \quad (\text{C29})$$

$$\tilde{\phi}_3^{d4} = h_{20} + h_{22} \quad (\text{C30})$$

$$= -\frac{9}{20}(3 + 7(A_1^u + V_1^d) - 56(\varphi^{002} - 2\varphi^{101} + \varphi^{200})), \quad (\text{C31})$$

$$\tilde{\phi}_3^{d5} = 2h_{22} \quad (\text{C32})$$

$$= -\frac{63}{10}(3 + 7(A_1^u + V_1^d) - 8(2\varphi^{002} + \varphi^{101} + 2\varphi^{200})). \quad (\text{C33})$$

Numerically one obtains for the COZ model [30]

$$\tilde{\phi}_3^{d1}(\mu = 1 \text{ GeV}) = 0.61, \quad (\text{C34})$$

$$\tilde{\phi}_3^{d2}(\mu = 1 \text{ GeV}) = 3.7. \quad (\text{C35})$$

This agrees with the numbers quoted in [16]. Using the lattice calculation we get

$$\tilde{\phi}_3^{d1}(\mu = 1 \text{ GeV}) = 0.51, \quad (\text{C36})$$

$$\tilde{\phi}_3^{d2}(\mu = 1 \text{ GeV}) = 0.71. \quad (\text{C37})$$

Here again the pure QCD sum-rule calculation seems to overestimate the effects.

#### APPENDIX D: MODELS FOR THE LEADING-TWIST NUCLEON DISTRIBUTION AMPLITUDE

In this section we present concrete models for the leading-twist nucleon distribution amplitude including next-to-next-to-leading conformal spin at the renormalization scale 1 GeV. At twist 3 one independent distribution amplitude  $\varphi(x_1, x_2, x_3, \mu)$  arises, see, e.g., [2]:

$$\varphi(x_1, x_2, x_3, \mu) = (V_1 - A_1)(x_1, x_2, x_3, \mu). \quad (\text{D1})$$

In [2] this distribution amplitude was denoted by  $\Phi_3(x_1, x_2, x_3, \mu)$ . From  $\varphi$  one easily gets  $V_1$ ,  $A_1$ , and  $T_1$ , see, e.g., [2]:

$$T_1(x_1, x_2, x_3) = \frac{1}{2}[\varphi(x_1, x_3, x_2) + \varphi(x_2, x_3, x_1)], \quad (\text{D2})$$

$$V_1(x_1, x_2, x_3) = \frac{1}{2}[\varphi(x_1, x_2, x_3) + \varphi(x_2, x_1, x_3)], \quad (\text{D3})$$

$$A_1(x_1, x_2, x_3) = \frac{1}{2}[\varphi(x_2, x_1, x_3) - \varphi(x_1, x_2, x_3)]. \quad (\text{D4})$$

The asymptotic form—only the leading conformal spin contribution—of  $\varphi(x_1, x_2, x_3, \mu)$  reads

$$\varphi_{\text{Asy}}(x_1, x_2, x_3, \mu) = 120x_1x_2x_3\phi_3^0(\mu), \quad (\phi_3^0 \equiv f_N). \quad (\text{D5})$$

Including next-to-leading conformal spin one gets [2]

$$\varphi(x_1, x_2, x_3, \mu) = \varphi_{\text{Asy}}(x_1, x_2, x_3, \mu)[1 + \tilde{\phi}_3^-(\mu)(x_1 - x_2) + \tilde{\phi}_3^+(\mu)(1 - 3x_3)], \quad (\text{D6})$$

with

$$\tilde{\phi}_3^- = \frac{\phi_3^-}{\phi_3^0}, \quad \tilde{\phi}_3^+ = \frac{\phi_3^+}{\phi_3^0}. \quad (D7)$$

In the literature also second moments of the leading-twist distribution amplitude were determined with QCD sum rules [29,30,37]. With this information one can build models for  $\varphi(x_1, x_2, x_3)$  at a certain renormalization scale  $\mu$ , including next-to-next-to-leading conformal spin. We will use the model from [30]  $\varphi^{\text{COZ}}(x_1, x_2, x_3)$  and the model from [37]  $\varphi^{\text{KS}}(x_1, x_2, x_3)$ :

$$\varphi^{\text{COZ}}(x_1, x_2, x_3) = \varphi_{\text{Asy}}(x_1, x_2, x_3)[23.814x_1^2 + 12.978x_2^2 + 6.174x_3^2 + 5.88x_3 - 7.098], \quad (D8)$$

$$\varphi^{\text{KS}}(x_1, x_2, x_3) = \varphi_{\text{Asy}}(x_1, x_2, x_3)[20.16x_1^2 + 15.12x_2^2 + 22.68x_3^2 - 6.72x_3 + 1.68(x_1 - x_2) - 5.04]. \quad (D9)$$

Bolz and Kroll derived a very simple model using some experimental constraints [47]. Their model for the leading-twist distribution amplitude reads

$$\varphi^{\text{BK}}(x_1, x_2, x_3) = \frac{1}{2}\varphi_{\text{Asy}}(x_1, x_2, x_3)(1 + 3x_1). \quad (D10)$$

Based on the lattice calculations of  $\varphi^{100}$ ,  $\varphi^{001}$ ,  $\varphi^{101}$ ,  $\varphi^{200}$ , and  $\varphi^{002}$  in [3,4] and Eq. (C1) we have obtained the model

$$\begin{aligned} \varphi^{\text{LAT}}(x_1, x_2, x_3) = \varphi_{\text{Asy}}(x_1, x_2, x_3) &(-0.401 + 29.214x_1 \\ &- 44.542x_2 + 7.664x_3 + 12.561x_1x_2 \\ &+ 31.748x_1x_3 - 103.09x_2x_3 \\ &- 41.880x_1^2 + 92.958x_2^2 + 17.836x_3^2). \end{aligned} \quad (D11)$$

- 
- [1] V.L. Chernyak and A.R. Zhitnitsky, Phys. Rep. **112**, 173 (1984).
  - [2] V. Braun, R. J. Fries, N. Mahnke, and E. Stein, Nucl. Phys. **B589**, 381 (2000).
  - [3] M. Göckeler *et al.* (QCDSF Collaboration), Proc. Sci., LAT2007 (2007) 147 [arXiv:0710.2489].
  - [4] M. Göckeler *et al.*, Phys. Rev. Lett. **101**, 112002 (2008).
  - [5] V.M. Braun *et al.* (QCDSF Collaboration), Phys. Rev. D **79**, 034504 (2009).
  - [6] V.M. Braun, A. Lenz, and M. Wittmann, Phys. Rev. D **73**, 094019 (2006).
  - [7] V.L. Chernyak and A.R. Zhitnitsky, JETP Lett. **25**, 510 (1977).
  - [8] V.L. Chernyak and A.R. Zhitnitsky, Sov. J. Nucl. Phys. **31**, 544 (1980).
  - [9] V.L. Chernyak, A.R. Zhitnitsky, and V.G. Serbo, JETP Lett. **26**, 594 (1977).
  - [10] V.L. Chernyak, V.G. Serbo, and A.R. Zhitnitsky, Sov. J. Nucl. Phys. **31**, 552 (1980).
  - [11] A. V. Radyushkin, arXiv:hep-ph/0410276.
  - [12] A. V. Efremov and A. V. Radyushkin, Theor. Math. Phys. **42**, 97 (1980).
  - [13] A. V. Efremov and A. V. Radyushkin, Phys. Lett. **94B**, 245 (1980).
  - [14] G.P. Lepage and S.J. Brodsky, Phys. Lett. **87B**, 359 (1979).
  - [15] G.P. Lepage and S.J. Brodsky, Phys. Rev. D **22**, 2157 (1980).
  - [16] V.M. Braun, A. Lenz, N. Mahnke, and E. Stein, Phys. Rev. D **65**, 074011 (2002).
  - [17] I.I. Balitsky, V.M. Braun, and A. V. Kolesnichenko, Nucl. Phys. **B312**, 509 (1989).
  - [18] V.L. Chernyak and I.R. Zhitnitsky, Nucl. Phys. **B345**, 137 (1990).
  - [19] M.K. Jones *et al.* (Jefferson Lab Hall A Collaboration), Phys. Rev. Lett. **84**, 1398 (2000).
  - [20] O. Gayou *et al.*, Phys. Rev. C **64**, 038202 (2001).
  - [21] O. Gayou *et al.* (Jefferson Lab Hall A Collaboration), Phys. Rev. Lett. **88**, 092301 (2002).
  - [22] V. Punjabi *et al.*, Phys. Rev. C **71**, 055202 (2005).
  - [23] C.F. Perdrisat, V. Punjabi, and M. Vanderhaeghen, Prog. Part. Nucl. Phys. **59**, 694 (2007).
  - [24] V.M. Braun, A. Khodjamirian, and M. Maul, Phys. Rev. D **61**, 073004 (2000).
  - [25] Y. Aoki, C. Dawson, J. Noaki, and A. Soni, Phys. Rev. D **75**, 014507 (2007).
  - [26] Y. Aoki *et al.*, Phys. Rev. D **78**, 054505 (2008).
  - [27] M.-q. Huang and D.-W. Wang, Phys. Rev. D **69**, 094003 (2004).
  - [28] A.J. Lenz, AIP Conf. Proc. **964**, 77 (2007).
  - [29] V.L. Chernyak and I.R. Zhitnitsky, Nucl. Phys. **B246**, 52 (1984).
  - [30] V.L. Chernyak, A.A. Ogloblin, and I.R. Zhitnitsky, Z. Phys. C **42**, 569 (1989).
  - [31] M.A. Shifman, A.I. Vainshtein, and V.I. Zakharov, Nucl. Phys. **B147**, 385 (1979).
  - [32] V.M. Braun and A. Lenz, Phys. Rev. D **70**, 074020 (2004).
  - [33] P. Ball, V.M. Braun, and A. Lenz, J. High Energy Phys. **05** (2006) 004.
  - [34] P. Ball, V.M. Braun, and A. Lenz, J. High Energy Phys. **08** (2007) 090.
  - [35] V.M. Braun *et al.*, Phys. Rev. D **74**, 074501 (2006).
  - [36] P.A. Boyle *et al.* (UKQCD Collaboration), Phys. Lett. B **641**, 67 (2006).
  - [37] I.D. King and C.T. Sachrajda, Nucl. Phys. **B279**, 785 (1987).
  - [38] B.L. Ioffe, Nucl. Phys. **B188**, 317 (1981).
  - [39] Y. Chung, H. G. Dosch, M. Kremer, and D. Schall, Nucl. Phys. **B197**, 55 (1982).
  - [40] V.M. Belyaev and B.L. Ioffe, Sov. Phys. JETP **56**, 493 (1982).

- (1982).
- [41] D. B. Leinweber, *Ann. Phys. (N.Y.)* **198**, 203 (1990).
- [42] B. L. Ioffe, *Prog. Part. Nucl. Phys.* **56**, 232 (2006).
- [43] M. Jamin, *Z. Phys. C* **37**, 635 (1988).
- [44] A. Lenz, M. Wittmann, and E. Stein, *Phys. Lett. B* **581**, 199 (2004).
- [45] G. Martinelli and C. T. Sachrajda, *Phys. Lett. B* **217**, 319 (1989).
- [46] T. Kaltenbrunner, M. Göckeler, and A. Schäfer, *Eur. Phys. J. C* **55**, 387 (2008).
- [47] J. Bolz and P. Kroll, *Z. Phys. A* **356**, 327 (1996).
- [48] To be precise, we have determined  $\phi^{002}$ ,  $\phi^{101}$ , and  $\phi^{110}$  from the BLW description and  $\phi^{200}$ ,  $\phi^{020}$ , and  $\phi^{011}$  from momentum conservation.
- [49] Z.-G. Wang, S.-L. Wan, and W.-M. Yang, *Phys. Rev. D* **73**, 094011 (2006).
- [50] Z.-G. Wang, S.-L. Wan, and W.-M. Yang, *Eur. Phys. J. C* **47**, 375 (2006).
- [51] T. M. Aliev and M. Savci, *Phys. Rev. D* **75**, 045006 (2007).
- [52] T. M. Aliev and M. Savci, *Phys. Lett. B* **656**, 56 (2007).
- [53] T. M. Aliev, K. Azizi, A. Ozpineci, and M. Savci, *Phys. Rev. D* **77**, 114014 (2008).
- [54] V. M. Braun, A. Lenz, G. Peters, and A. V. Radyushkin, *Phys. Rev. D* **73**, 034020 (2006).
- [55] J. Rohrwild, *Phys. Rev. D* **75**, 074025 (2007).
- [56] T. M. Aliev, K. Azizi, and A. Ozpineci, *Nucl. Phys. A* **799**, 105 (2008).
- [57] V. M. Braun *et al.*, arXiv:0902.3087.
- [58] V. M. Braun, D. Y. Ivanov, A. Lenz, and A. Peters, *Phys. Rev. D* **75**, 014021 (2007).
- [59] V. M. Braun, D. Y. Ivanov, and A. Peters, *Phys. Rev. D* **77**, 034016 (2008).
- [60] V. M. Braun, D. Y. Ivanov, A. Lenz, and A. Peters, arXiv:0901.3184.
- [61] M.-Q. Huang and D.-W. Wang, arXiv:hep-ph/0608170.
- [62] Z. G. Wang, *J. Phys. G* **34**, 493 (2007).
- [63] Y.-m. Wang, Y. Li, and C.-D. Lu, *Eur. Phys. J. C* **59**, 861 (2009).
- [64] Y.-L. Liu and M.-Q. Huang, *Nucl. Phys. A* **821**, 80 (2009).
- [65] Y.-L. Liu, M.-Q. Huang, and D.-W. Wang, arXiv:0810.4973.
- [66] K. Passek-Kumericki and G. Peters, *Phys. Rev. D* **78**, 033009 (2008).
- [67] L. Andivahis *et al.*, *Phys. Rev. D* **50**, 5491 (1994).
- [68] R. C. Walker *et al.*, *Phys. Rev. D* **49**, 5671 (1994).
- [69] J. Litt *et al.*, *Phys. Lett.* **31B**, 40 (1970).
- [70] C. Berger, V. Burkert, G. Knop, B. Langenbeck, and K. Rith, *Phys. Lett.* **35B**, 87 (1971).
- [71] T. Janssens, R. Hofstadter, E. B. Hughes, and M. R. Yearian, *Phys. Rev.* **142**, 922 (1966).
- [72] M. E. Christy *et al.* (E94110 Collaboration), *Phys. Rev. C* **70**, 015206 (2004).
- [73] I. A. Qattan *et al.*, *Phys. Rev. Lett.* **94**, 142301 (2005).
- [74] W. Bartel *et al.*, *Nucl. Phys.* **B58**, 429 (1973).
- [75] L. E. Price *et al.*, *Phys. Rev. D* **4**, 45 (1971).
- [76] J. Arrington, *Phys. Rev. C* **68**, 034325 (2003).
- [77] C. B. Crawford *et al.*, *Phys. Rev. Lett.* **98**, 052301 (2007).
- [78] B. D. Milbrath *et al.* (Bates FPP Collaboration), *Phys. Rev. Lett.* **80**, 452 (1998).
- [79] T. Pospischil *et al.* (A1 Collaboration), *Eur. Phys. J. A* **12**, 125 (2001).
- [80] M. Jones (private communication).
- [81] A. Lung *et al.*, *Phys. Rev. Lett.* **70**, 718 (1993).
- [82] G. Kubon *et al.*, *Phys. Lett. B* **524**, 26 (2002).
- [83] H. Anklin *et al.*, *Phys. Lett. B* **428**, 248 (1998).
- [84] R. Madey *et al.* (E93-038 Collaboration), *Phys. Rev. Lett.* **91**, 122002 (2003).
- [85] W. Xu *et al.*, *Phys. Rev. Lett.* **85**, 2900 (2000).
- [86] W. Xu *et al.* (Jefferson Lab E95-001 Collaboration), *Phys. Rev. C* **67**, 012201 (2003).
- [87] H. Anklin *et al.*, *Phys. Lett. B* **336**, 313 (1994).
- [88] H. Zhu *et al.* (E93026 Collaboration), *Phys. Rev. Lett.* **87**, 081801 (2001).
- [89] D. Rohe *et al.*, *Phys. Rev. Lett.* **83**, 4257 (1999).
- [90] C. Herberg *et al.*, *Eur. Phys. J. A* **5**, 131 (1999).
- [91] M. Ostrick *et al.*, *Phys. Rev. Lett.* **83**, 276 (1999).
- [92] J. Becker *et al.*, *Eur. Phys. J. A* **6**, 329 (1999).
- [93] T. Eden *et al.*, *Phys. Rev. C* **50**, R1749 (1994).
- [94] B. Plaster *et al.* (Jefferson Laboratory E93-038 Collaboration), *Phys. Rev. C* **73**, 025205 (2006).
- [95] E. Geis *et al.* (BLAST Collaboration), *Phys. Rev. Lett.* **101**, 042501 (2008).
- [96] D. I. Glazier *et al.*, *Eur. Phys. J. A* **24**, 101 (2005).
- [97] G. Warren *et al.* (Jefferson Lab E93-026 Collaboration), *Phys. Rev. Lett.* **92**, 042301 (2004).
- [98] J. Bermuth *et al.*, *Phys. Lett. B* **564**, 199 (2003).
- [99] I. Passchier *et al.*, *Phys. Rev. Lett.* **82**, 4988 (1999).
- [100] J. Golak, G. Ziemer, H. Kamada, H. Witala, and W. Gloeckle, *Phys. Rev. C* **63**, 034006 (2001).
- [101] R. Schiavilla and I. Sick, *Phys. Rev. C* **64**, 041002 (2001).
- [102] S. Galster *et al.*, *Nucl. Phys.* **B32**, 221 (1971).
- [103] J. J. Kelly, *Phys. Rev. C* **70**, 068202 (2004).
- [104] A. Bodek, S. Avvakumov, R. Bradford, and H. Budd, *Eur. Phys. J. C* **53**, 349 (2008).
- [105] P. Stoler, *Phys. Rep.* **226**, 103 (1993).
- [106] L. M. Stuart *et al.*, *Phys. Rev. D* **58**, 032003 (1998).
- [107] W. Bartel *et al.*, *Phys. Lett.* **28B**, 148 (1968).
- [108] S. Stein *et al.*, *Phys. Rev. D* **12**, 1884 (1975).
- [109] F. Foster and G. Hughes, *Rep. Prog. Phys.* **46**, 1445 (1983).
- [110] S. S. Kamalov, S. N. Yang, D. Drechsel, O. Hanstein, and L. Tiator, *Phys. Rev. C* **64**, 032201 (2001).
- [111] J. C. Alder *et al.*, *Nucl. Phys.* **B46**, 573 (1972).
- [112] V. V. Frolov *et al.*, *Phys. Rev. Lett.* **82**, 45 (1999).
- [113] K. Joo *et al.* (CLAS Collaboration), *Phys. Rev. Lett.* **88**, 122001 (2002).
- [114] V. M. Braun, A. N. Manashov, and J. Rohrwild, *Nucl. Phys.* **B807**, 89 (2009).
- [115] M. Bergmann and N. G. Stefanis, arXiv:hep-ph/9403210.
- [116] M. Bergmann, W. Schroers, and N. G. Stefanis, *Phys. Lett. B* **458**, 109 (1999).
- [117] V. M. Braun, S. E. Derkachov, G. P. Korchemsky, and A. N. Manashov, *Nucl. Phys.* **B553**, 355 (1999).